To the Graduate Council:

I am submitting herewith a thesis written by David Christopher Modeste entitled "Evaluation of Improved Anion-Exchange Resin-Based Seed Regeneration Concept for Coal Fired MHD Power System." I have examined the final copy of this thesis for form and content and recommend that it be accepted in partial fulfillment of the requirements for the Master of Science degree with a major in Chemical Engineering.

Atul C. Sheth

Atul C. Sheth, Major Professor

We have read this thesis
and recommend its acceptance:

Clayde W Campbell

Roy J. Schulz

Accepted for the Council:

Lewinkel

Vice Provost
and Dean of the Graduate School

STATEMENT OF PERMISSION TO USE

In presenting this thesis in partial fulfillment of the requirements for a Master's degree at The University of Tennessee, Knoxville, I agree that the Library shall make it available to borrowers under rules of the Library. Brief quotations from this thesis are allowable without special permission, provided that accurate acknowledgment of source is made.

Permission for extensive quotation from or reproduction of this thesis may be granted by my major professor, or in his absence, by the Head of Interlibrary Services when, in the opinion of either, the proposed use of the material is for scholarly purposes. Any copying or use of the material in this thesis for financial gain shall not be allowed without my written permission.

Signature David C. Hodest

Date 28th November, 1988

EVALUATION OF IMPROVED ANION-EXCHANGE RESIN-BASED SEED REGENERATION CONCEPT FOR COAL FIRED MHD POWER SYSTEM

A Thesis

Presented for the

Master of Science

Degree

The University of Tennessee, Knoxville

David Christopher Modeste

December 1988

To My Beloved Mother

Jane Elizabeth Modeste

"Love conquers all"

ACKNOWLEDGEMENTS

The author would like to express his sincere appreciation and thanks to Dr. Atul Sheth, his major professor and chairman of the thesis committee for his continuous assistance and guidance during this work. Special thanks are also extended to committee members Dr. Lloyd Crawford, and Dr. Roy Schulz for taking time to read and correct the manuscript.

Sincere thanks are extended to Mr. Phillip Sherrill, Mrs. Birdie Farris, Ms. Kathy Parks and Ms. Teresa Sloan of the UTSI Chemistry Laborotary for their assistance in the laboratory.

The author also wishes to express his gratitude and appreciation to Mr. Bob Douglas, Mr. Bill Hardison and Mr. James Knight of the Energy Conversion Programs at UTSI for their assistance with the design and construction of the experimental apparatus.

The author is indebted to his family for their constant support and encouragement. Without them, this work would not have been possible.

ABSTRACT

Application of the technology of Magnetohydrodynamics (MHD) to coal fired power plants can result in higher overall efficiencies than those shown by conventional coal fired power plants. Coal-fired MHD power plants require the use of a seed material to make the combustion gases electrically conducting, and this results in an inherent sulfur removal process which makes such plants environmentally atttractive. In order for the MHD technology to be economically feasible, an efficient method of recovery, regeneration, and recycle of the spent seed material must be found. To accomplish this task, Butler (UTSI 1986) investigated an ion-exchange resin-based seed regeneration concept and also identified a fixed-bed sorption model of Selke and Bliss to satisfy the experimental breakthrough behavior of an ion-exchange system. The Selke and Bliss fixed bed model assumes liquid-film diffusion control and a non-linear equilibrium isotherm. This study extended the work done by Butler by using a model developed by Antonson which assumes particle diffusion control with non-linear equilibrium . In addition, the ion-exchange experiments were done under CO_2 pressure in an effort to combine the resin exhaustion and carbonation steps, and also to see if an an increase in resin capacity would occur. Results from a series of fixed bed experiments verified that the equilibrium of the sulfate- bicarbonate exchange system was non-linear. The results also showed that at higher CO_2 pressures, the equilibrium capacity of the system was increased. Finally, results obtained from the mathematical model used to describe the sulfate-bicarbonate system compare favorably with the experimental results.

TABLE OF CONTENTS

CHAPTER PAGE

I. INTRODUCTION 1

MHD Background 1

Ion-Exchange Resin-Based Seed Regeneration Concept 4

II. LITERATURE REVIEW 9

III. THEORY 12

Equilibrium Relationships 15

Rate Controlling Mechanisms 19

Mathematical Model 21

IV. EXPERIMENTAL EQUIPMENT AND PROCEDURE 25

Apparatus 25

Experimental Procedure 28

V. RESULTS AND DATA EVALUATION 32

Experimental Breakthrough Curves 32

Determination of Equilibrium Capacity 36

Determination of Equilibrium Isotherm 38

Determination of Diffusion Coefficients 43

VI. DISCUSSION OF RESULTS 47
Equilibrium Data 47
Diffusion Coefficients 50
Mathematical Model 51

VII. PROCESS DESIGN AND ECONOMICS 59
Material Balance 59
Preliminary Economics 64
Comparison With Existing Processes 69

VIII. CONCLUSIONS AND RECOMMENDATIONS 73
Recommendations 74

LIST OF REFERENCES 76

APPENDIXES 80
APPENDIX A. COMPUTER SCHEME 81
APPENDIX B. COMPUTER PROGRAMS 87
APPENDIX C. EXPERIMENTAL DATA 92

VITA 97

LIST OF TABLES

TABLE PAGE

I. Physical Characteristics of Amberlite IRA-67 27

II. Conditions used for Fixed-bed Experiments 33

III. Data used for Equilibrium Isotherm Calculations 40

IV. Langmuir Constants 42

V. Diffusion Coefficients from Best Fit of Experimental Breakthrough Curves 46

VI. Comparison of Diffusion Coefficients with Literature Values 52

VII. Design Basis for Proposed Seed Regeneration Plant 60

VIII. Chemical Composition of the Spent Seed Extract 62

IX. Summary of Material Balance Calculations for Resin Exhaustion . . . 65

X. Summary of Material Balance Calculations for Resin Regeneration . . 66

XI. Assumptions for Material Balance and Cost Analysis 67

XII. Initial Capital Costs for the Proposed Seed Regeneration Plant . . . 68

XIII. Annual Operating Costs for the Proposed Seed Regeneration Plant . . 70

XIV. Comparison of Economics for Candidate Seed Regeneration Processes . 72

LIST OF FIGURES

FIGURE PAGE

1. Coal-Fired flow facility at UTSI 2
2. Seed regeneration system with two-step regeneration 6
3. Modified seed regeneration system with one-step regeneration 7
4. Typical breakthrough curve for a fixed bed system 13
5. Differential material balance around fixed bed 14
6. Description of typical equilibrium curves 17
7. Schematic diagram of experimental apparatus 26
8. Reproducibility check of run IEX-2 29
9. Reproducibility check of run IEX-7 30
10. Reproducibility check of Butler's data 31
11. Experimental breakthrough curves for runs IEX-1 – IEX-4 34
12. Experimental breakthrough curves for runs IEX-5 – IEX-8 35
13. Plot of $(1 - \frac{C}{C_o})$ vs. t for run IEX-1 37
14. Fit of linearized Langmuir isotherm to experimental data 39
15. Comparison of equilibrium isotherms with experimental data 41

16. Theoretical breakthrough curves obtained from Antonson's model . . 45

17. Comparison of Equilibrium Isotherms at various CO_2 pressures . . . 49

18. Match of experimental and theoretical breakthrough curves for run IEX-2: Match at $a_2C_o = 13.72$, $X^* = 12.00$ 54

19. Match of experimental and theoretical breakthrough curves for run IEX-5: Match at $a_2C_o = 1.42$, $X^* = 0.95$ 55

20. Match of experimental and theoretical breakthrough curves for run IEX-6: Match at $a_2C_o = 5.32$, X^* =4.8 56

21. Match of experimental and theoretical breakthrough curves for run IEX-8: Match at $a_2C_o = 17.76$, $X^* = 16.00$ 57

22. Schematic diagram of proposed seed regeneration plant 61

LIST OF SYMBOLS

a_1: first Langmuir constant (dimensionless)

a_2: second Langmuir constant (ml./gm.)

C: concentration of SO_4^{2-} (gm./ml.)

C_o: initial concentration of K_2SO_4 (gm. SO_4^{2-}/ml)

C_s: sulfate concentration at fluid-solid interface (gm. SO_4^{2-}/ml)

D: intraparticle diffusion coefficient (cm^2/sec)

K: defined by equation (15)

k_la: film diffusion coefficient (cm./sec.)

$\overline{K}$: defined by equation (10)

K_o: equilibrium constant at equilibrium conditions (diminsionless)

m: ratio of void fraction to particle fraction (dimensionless)

$q(z,t)$: average solid phase concentration in the particle (gm. SO_4^{2-}/ml)

$q_i(r,z,t)$: solid phase concentration in the particle (gm. SO_4^{2-}/ml)

$q_s(R,z,t)$: solid phase concentration at the fluid-solid interface (gm. SO_4^{2-}/ml)

q_∞: equilibrium concentration in the particle (gm. SO_4^{2-}/ml)

r: radial coordinate in spherical particles (cm.)

R: spherical radius of particles (cm.)

t: time (sec.)

v: linear velocity in the packed bed (cm./sec.)

V: volumetric flowrate of solution (ml./sec.)

V_R: volume of resin (cm^3)

X: z/mv (sec.)

X^*: $3Da_1z/mvR^2$ (dimensionless)

z: column position (cm.)

γ_n: activity coefficient of the nth species (dimensionless)

λ: dummy variable of integration

ϕ: C/C_o (dimensionless)

ρ: particle density (gm./cm^3)

θ: (t - z/v) (sec.)

θ^*: $(2D/R^2)(t - z/v)$ (sec.)

μ: molecular weight of SO_4^{2-} ion 96.06 gms./gm-mole

CHAPTER I

INTRODUCTION

MHD Background

The University of Tennessee Space Institute (UTSI) is currently involved in research on the open-cycle, coal-fired magnetohydrodynamics (MHD) power system. In the MHD technology, hot combustion gases at temperatures up to $5000^{o}F$ are seeded with a potassium salt, usually potassium carbonate (K_2CO_3), which increases the electrical conductivity of the gases due to thermal ionization of the potassium. The electrically conductive plasma is then passed through a magnetic field which generates an electrical potential. Generated DC current is then tapped from the system via electrodes installed in the channel duct. Further downstream of the MHD channel, electricity is generated via the conventional steam-turbine/generator set up [1]. The generation of this additional electricity begins after the hot combustion gases leave the MHD diffuser. At this point, the gases are passed through a radiant furnace and secondary combustor and subsequently through the Superheater Test Module where superheated steam is produced. The Superheater Test Module is not a unit which would be in a commercial MHD plant. Such a unit might be replaced by other heat recovery devices in the commercial plant for the production of superheated steam. Other downstream components in the MHD system include either a baghouse, an electrostatic precipitator or a venturi scrubber, which are operated in parallel to capture spent seed material and flyash. The MHD facility at UTSI is an experimental facility which is equipped with all of the items mentioned above. Figure 1 gives a

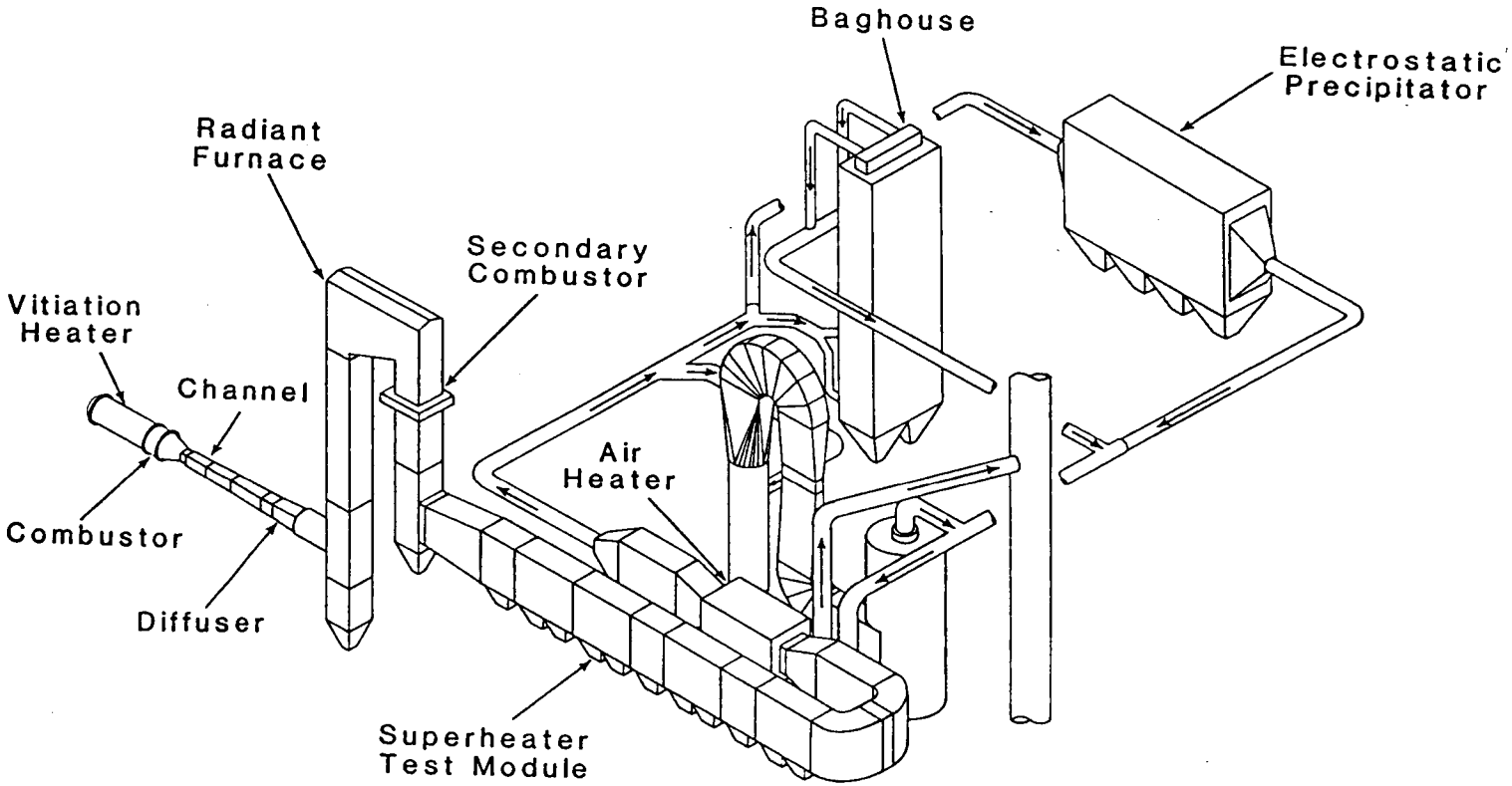


Figure 1. Coal-Fired flow facility at UTSI.

description of the MHD set up at UTSI.

The MHD technology has some built in advantages which make it an attractive energy conversion system. Seeding the coal feedstock with potassium salts such as K_2CO_3 increases the electrical conductivity of the combustion products and also allows for the removal of potentially harmful sulfur containing compounds. These compounds, if released into the atmosphere, could act as a precursor to acidic species believed to be harmful to the environment.

Efficient recovery and regeneration of the spent seed is vital to the MHD system because it contains large quantities of soluble potassium which, if recovered, can be returned to the system for further use and also improve the overall economics and environmental acceptability of the system. Most of the recoverable potassium (K_2SO_4) is collected along with the flyash particles in the particulate collection devices such as the electrostatic precipitator and the baghouse filter. For recycle and reuse, potassium from such a mixture of spent seed needs to be quantitatively recovered and regenerated or desulfurized to a sulfur-free form. This step of sulfur removal is called seed regeneration.

There are several processes available which can be used to separate sulfur from alkali metal sulfates. These separation processes can be divided into two groups: (1) Those which recover sulfur in a commercially usable form, and (2) those which recover sulfur in a disposable form. Processes such as PERC, Aqueous Carbonate, Modified Tampella, and Westinghouse can be grouped in the first category; while, the second category includes double decomposition precipitation type processes that include the Engle Precht, Formate, Econoseed and Double Alkali Process. All of these processes have some disadvantages such as high capital costs or excessive energy requirements which make them less attractive as possible seed regeneration processes for the MHD system [2].

A seed regeneration system applicable to MHD plants would have to meet certain criteria. These criteria include being economically feasible, having low energy requirements and a high yield of potassium for recycle to the MHD power plant. In order to develop such a system, work was started at UTSI (Butler 1986) to test the feasibility of an ion-exchange resin-based seed regeneration process. Results from the preliminary bench scale evaluation, carried out by Butler, verified that such a concept is technically feasible and can be adapted for use in MHD power plants if suitably developed.

Ion-Exchange Resin-Based Seed Regeneration Concept

In the ion-exchange resin-based seed regeneration concept, the potassium sulfate containing solution is passed through a column packed with anion-exchange resins. The resin, Amberlite IRA-68, is a weakly basic anion-exchange resin with high porosity and contains tertiary amine functional groups. Amberlite IRA-68 has a strong affinity for hydroxide ions and its affinity for other anions decreases in the following order [12]:

$$OH^- \longrightarrow PO_4^{3-} \longrightarrow SO_4^{2-} \longrightarrow NO_3^- \longrightarrow Cl^- \longrightarrow HCO_3^-$$

For the seed regeneration system, SO_4^{2-} ions are to be removed from the K_2SO_4 solution. To accomplish this, the resin, which is supplied with hydroxide ions occupying the active sites must be converted to the bicarbonate form so that it can be exchanged with the sulfate ions. Equation (1) describes the balance achieved in the carbonation of the hydroxide form of the resin, but not the actual chemical mechanism involved in the activation of the resin.

$$ROH + CO_2 \longrightarrow RHCO_3 \quad (1)$$

After the resin is converted to the bicarbonate form, it can then be exhausted by the K_2SO_4 as shown in equation (2).

$$2RHCO_3 + K_2SO_4 \longrightarrow R_2SO_4 + 2KHCO_3 \quad (2)$$

The recovered potassium bicarbonate can then be returned to the MHD combustor for reuse after further concentration and drying. To facilitate further use, the resin must be regenerated. This can be done by treating the resin with a solution of ammonium hydroxide [1].

$$R_2SO_4 + 2NH_4OH \longrightarrow (NH_4)_2SO_4 + 2ROH \quad (3)$$

The ammonium sulfate can be recovered and sold as fertilizer, or, as shown in equation (4), converted to ammonium hydroxide using $Ca(OH)_2$. These resin exhaustion and regeneration steps are outlined in Figure 2.

$$Ca(OH)_2 + (NH_4)_2SO_4 \longrightarrow CaSO_4 + 2NH_4OH \quad (4)$$

The process outlined above is descriptive of the work done by Butler in his bench-scale evaluation of the ion-exchange resin-based seed regeneration process. This study extends Butler's work by making two major modifications to his original concept. The first modification was to carry out the exhaustion step, equation (2), under moderate CO_2 pressure as described in Figure 3. Placing the exhaustion column under moderate CO_2 pressure during the exhaustion steps decreases the number of steps required to convert the resin to the bicarbonate form from two to one. This reduction occurs because placing the column under CO_2

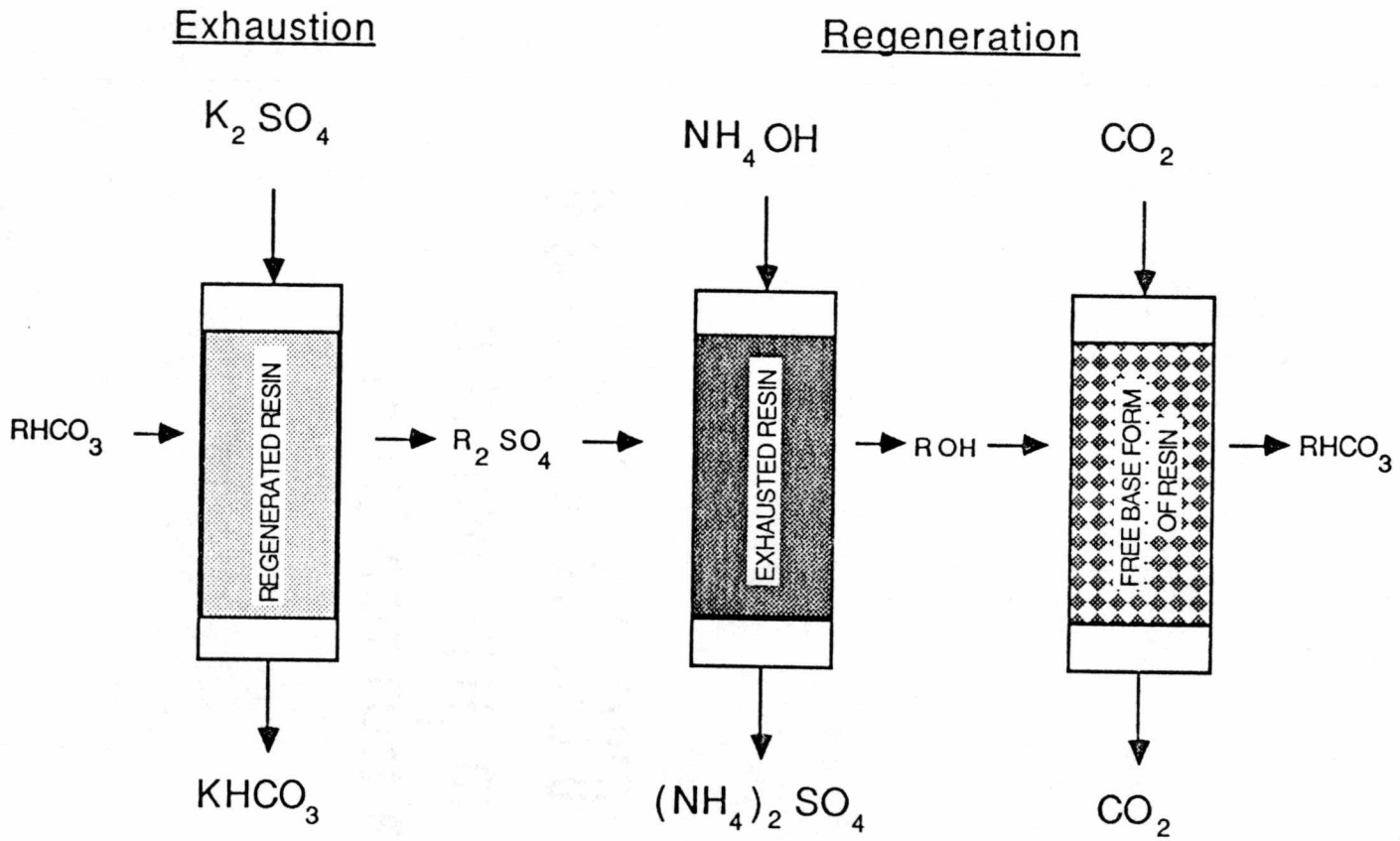


Figure 2. Seed regeneration system with two-step regeneration.

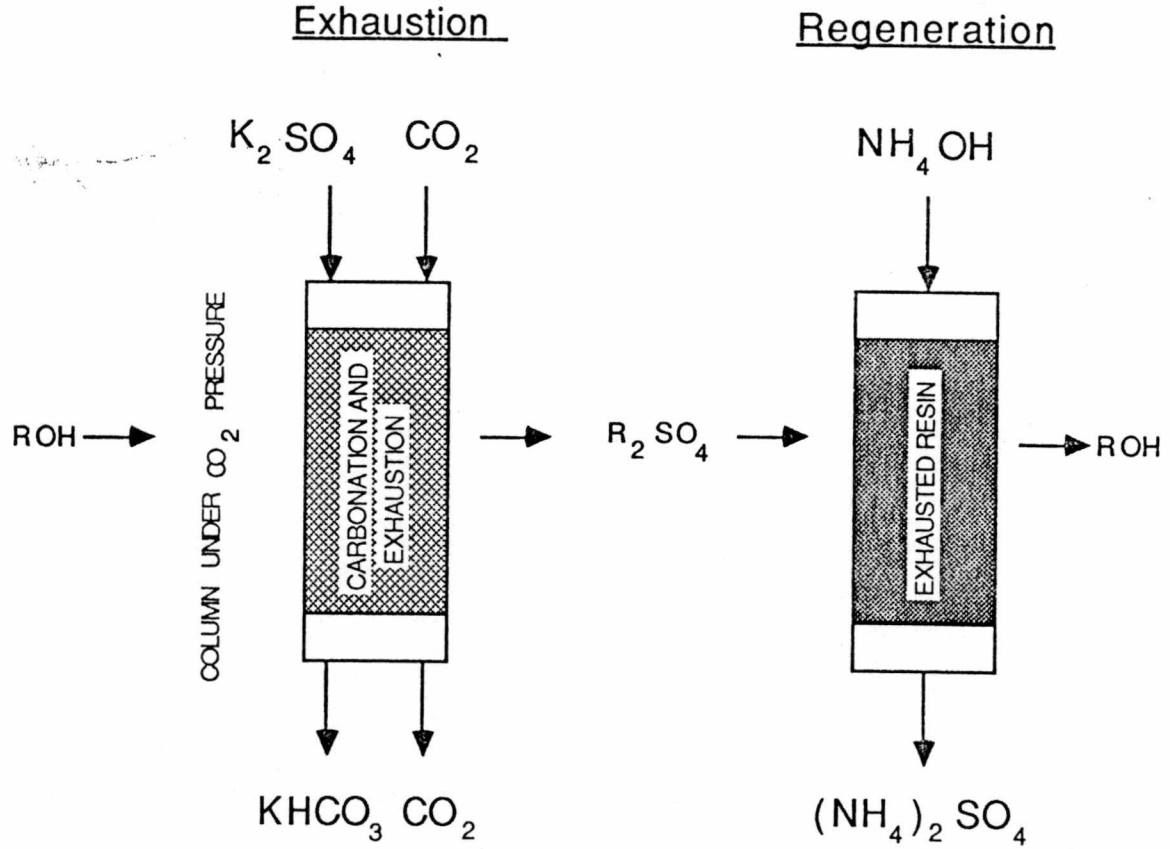


Figure 3. Modified seed regeneration system with one-step regeneration

pressure, effectively combines the last step of the resin regeneration cycle equation (1) with the exhaustion step equation (2). Furthermore, carrying out the exhaustion step under CO_2 pressure also increases the amount of active HCO_3^- sites available for ion-exchange. The second modification includes the selection of a proper mathematical model that allows for effects due to solid phase diffusion. This modification comes as a direct result of Butler's findings suggesting that solid diffusion was probably a rate contributing factor during the final stages of the resin exhaustion cycle. This second modification should provide a better prediction of the tail-end characteristics of the experimental breakthrough curve.

CHAPTER II

LITERATURE REVIEW

Ion-exchange techniques can be applied in situations where separation of a single or select group of ions from a solution is required. Applications of ion-exchange based techniques range from water softening and recovery of precious metals to separation of amino acids. Several researchers [3], [4], [6], [8], have investigated the characteristics of ion-exchange systems similar to those mentioned above; however, a few [2], [12], have looked at ion-exchange as it applies to the regeneration of spent seed material from MHD power plants. Fortunately, the available literature contains ample information about the experimental and analytic methods used in the investigation of ion-exchange systems which can be applied to this study.

There are several factors that must be considered when investigating an ion-exchange system. These include equilibrium considerations, mass transfer effects, and economic feasibility. A large number of researchers have focused their efforts on determining the effects of equilibrium and mass transfer effects on ion-exchange systems. Work has been done by Rosen [5] on the general problem of the transient behavior of a fixed bed sorption system with a linear equilibrium where the rate of adsorption is determined by the combined effect of diffusion through the liquid film and diffusion into the spherical resin particles. The mathematical model which Rosen developed considered a linear equilibrium isotherm of the form:

$$q_s = KC \tag{5}$$

where K is equilibrium constant for the exchange reaction and q_s is the concentra-

tion of exchanged ion on the resin surface in equilibrium with C, the concentration of sorbate in the solution . Rosen's choice of a linear equilibrium isotherm, resulted in a linear set of equations for describing the mathematical model. Based on these equations, he derived an exact solution for the system under linear equilibrium. The assumption that the exchange system exhibits a linear equilibrium has been shown to be valid in many ion-exchange systems where the equilibrium is governed by monovalent-monovalent exchanges and the solution concentration is sufficiently low. For situations where the exchanging ions are transferred by divalent-monovalent exchanges, as in this study, Selke and Bliss [26] have concluded that such systems tend to follow a non-linear type equilibrium isotherm.

Ion-exchange systems which have non-linear equilibrium relationships are particularly difficult to model because analytical solutions for this type of problem are probably not possible. Tien and Thodos [7] have developed a model for this case using numerical methods. The non-linear equilibrium in their case was described by the Freundlich type of adsorption isotherm given by:

$$q_s = AC_o^a \tag{6}$$

where a and A are constants, and C_o is the initial adsorbate concentration. In addition to a non-linear equilibrium relationship, Tien and Thodos also consider the combined effects of film diffusion and solid phase diffusion. Butler [1] has applied a model developed by Selke and Bliss [26] for a non-linear Langmuir-type equilibrium given by:

$$q_s = \frac{a_1 C_o}{1 + a_2 C_o} \tag{7}$$

where a_1 and a_2 are constants. Butler assumed that liquid-film diffusion was the controlling mass transfer mechanism. A more extensive study based on a Langmuir type non-linear equilibrium has been developed by Antonson [9]. In

his work, Antonson considered the effect of solid phase diffusion on the exchange rate of ethane in a fixed bed system employing type 4A molecular sieves. The resulting mathematical expression developed to describe this system was in the form of a non-linear partial differential equation which was then solved using numerical methods.

Thomas [10] has developed analytic results for the ion-exchange system based on a reaction rate controlled mass transfer mechanism and a linear equilibrium relationship. His model was further extended by Heister and Vermuelen [11] to include a non-linear case. As a result of his work a set of generalized curves were developed which gave the concentration $\frac{C}{C_o}$ as a function of time with the equilibrium constant **r** as a parameter. These generalized curves can be applied to the design of fixed bed systems as long as the pertinent data, such as the equilibrium parameter **r** for the system are available.

CHAPTER III

THEORY

The exchange of ions between a flowing liquid stream with ion A and a solid particle phase containing ion B involves transients in both the fluid and solid phases. This task can be accomplished in several ways: (1) Batch operation, (2) fixed bed operation, (3) Stagewise operation. Fixed bed operation is the most common technique used with this type of system [13]. In this case, the solid phase consists of molecular sieves, natural zeolites, or ion-exchange resins. The resin is usually subjected to a step change in solution of known concentration in the exchanging ion. As the liquid front moves through the bed, the concentration of the resin phase increases until it is in equilibrium with the surrounding fluid. The change in the concentration of the liquid phase is described by the concentration history or "breakthrough curve", which gives the concentration of the eluent as a function of time or volume of liquid passed through the column. A typical breakthrough curve for a fixed bed system is shown in Figure 4. The breakpoint described in this figure is the point where the first noticeable change in the concentration of the eluent is observed. A quantitative description of the ion-exchange resin-based process can be obtained by doing a differential material balance over a differential slice of the fixed bed. If the resin particle is assumed to be spherical in shape, and the flow rate is considered constant through the bed (plug flow), a differential material balance around the cross-section of the bed (Figure 5) would yield.

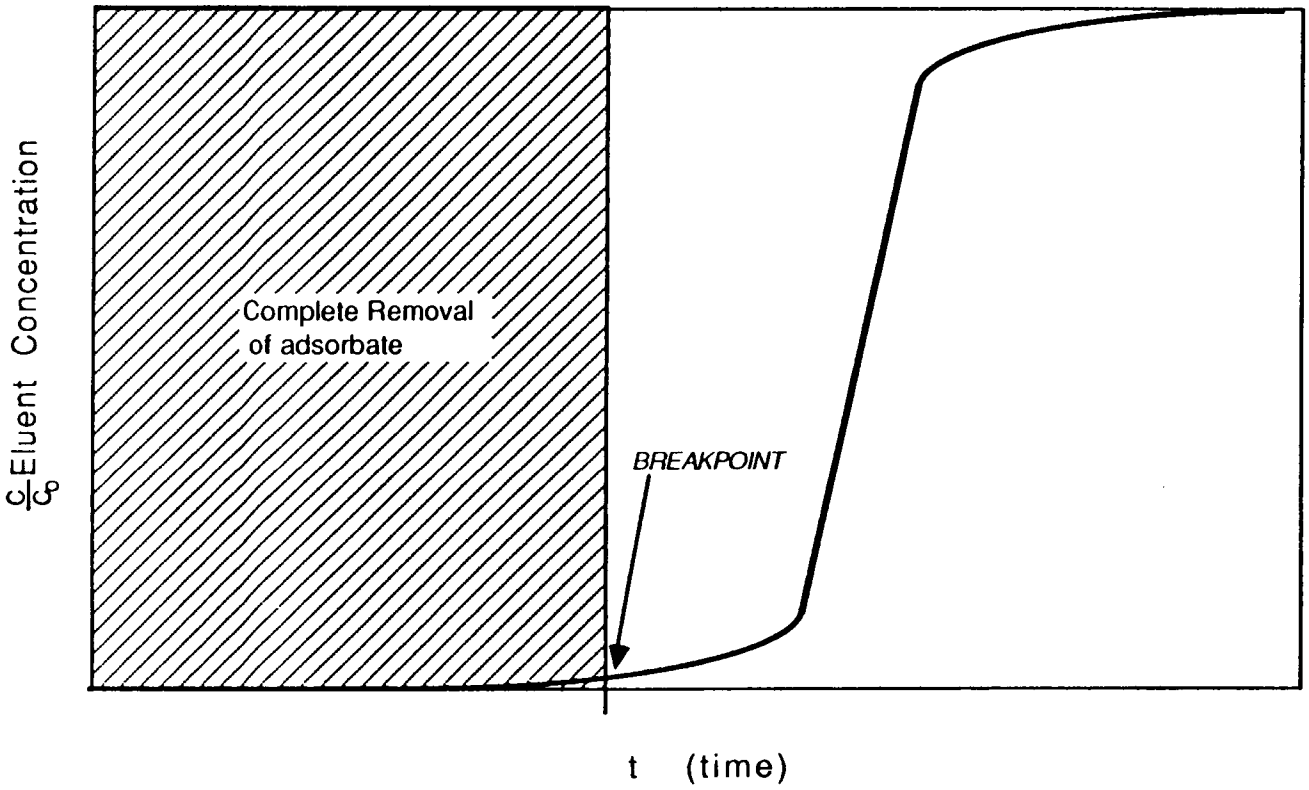


Figure 4. Typical breakthrough curve for a fixed bed system

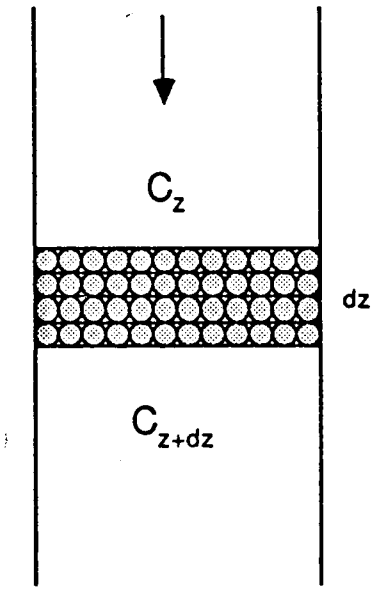


Figure 5. Differential material balance around fixed bed

$$\left(\frac{\partial C}{\partial t}\right)_z + V\left(\frac{\partial C}{\partial z}\right)_t + \frac{1}{m}\left(\frac{\partial q}{\partial t}\right)_t = 0 \qquad (8)$$

Where C is the concentration of adsorbate in the liquid phase, V is the flowrate, t is the time, q is the concentration of adsorbate on the resin, m is the ratio of the void fraction to particle fraction in the packed bed, and z is the height of packing in the bed. Applying the proper equilibrium and mass transfer constraints would yield a solution to equation (8) which can then be used to predict the behavior of the fixed bed system. The constraints which apply to the system investigated in this work will be presented in subsequent sections.

Equilibrium Relationships

The behavior of fixed bed ion-exchange systems is affected by the nature of the equilibrium governing the ion-exchange process. Typically, there are four types of equilibrium behavior which can be identified in a fixed bed system [14]:

1. Irreversible equilibrium
2. Favorable equilibrium
3. Linear equilibrium
4. Unfavorable equilibrium

These four types of behavior represent distinct situations which occur in the ion-exchange process. In the first case, the equilibrium concentration in the resin, q_∞, is constant for all values of the initial concentration of the adsorbate. For the second case, the resin phase concentration is a function of the initial concentration and a plot of q_∞vs. C_o is usually concave upward in shape. Case 3 represents a special form of case 2 when the concentrations in the solid and liquid phases are directly proportional to each other. The slope of the linear plot in this case, is

the equilibrium constant K. Finally, case 4 describes the situation where the solid phase is releasing an ion to the liquid phase (desorption). In this case, a plot of q_∞ vs. C_o would be concave downward. Figure 6. gives a description of these four types of equilibrium isotherms.

In order to get a quantitative description of the equilibrium behavior of the sulfate-bicarbonate exchange system being studied, Butler [1] used the overall ion transfer reaction to obtain an expression for the equilibrium constant $\overline{K}$. The method he used to obtain $\overline{K}$ is described below:

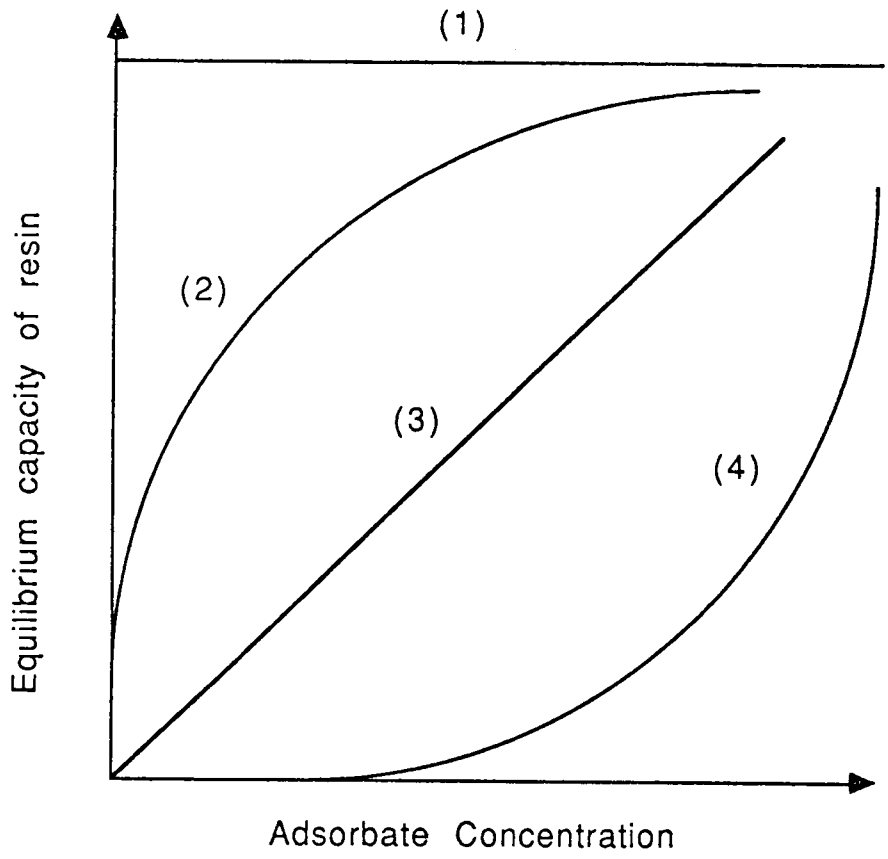
$$SO_4^{2-} + 2RHCO_3 \longrightarrow R_2SO_4 + 2HCO_3^- \tag{9}$$

The equilibrium constant for this exchange is then given by:

$$K_o = \frac{[R_2SO_4]\gamma_{R_2SO_4}[HCO_3^-]^2\gamma^2_{HCO_3^-}}{[SO_4^{2-}]\gamma_{SO_4^{2-}}[RHCO_3]^2\gamma^2_{RHCO_3}} \tag{10}$$

where terms in the brackets refer to solution concentration in moles per liter and γ's are respective activity coefficients. In dilute solution, it is assumed that the activity coefficients in the liquid phase approach unity. If the resin capacity at saturation is q_∞, ρ is the wet bulk density of the resin phase and C is the concentration in the bulk fluid, the concentration terms in equation (9) can be expressed as follows:

$$[R_2SO_4] = \frac{q\rho}{\mu}; \qquad [RHCO_3] = \frac{2(q_\infty - q)\rho}{\mu} \tag{11}$$



(1) Irreversible equilibrium

(2) Favorable equilibrium

(3) Linear equilibrium

(4) Unfavorable equilibrium

Figure 6. Description of typical equilibrium curves

where μ is the molecular weight of sulfate ions and q is the resin phase concentration at time t. Concentrations of $[SO_4^{2-}]$ and $[HCO_3^-]$ at any time t are related by equation (12) where C_o is the inital concentration of $[SO_4^{2-}]$.

$$[SO_4^{2-}] + \frac{1}{2}[HCO_3^-] = C_o \tag{12}$$

if,

$$[SO_4^{2-}] = C \tag{13}$$

The bicarbonate concentration is then given by:

$$[HCO_3^-] = 2(C_o - [SO_4^{2-}]) \tag{14}$$

Substitution of these terms into equation (9) along with the assumption that the liquid phase activity coefficients approach unity in dilute solution will yield the following non-equilibrium relationship.

$$K = K_o \frac{\gamma_{HCO_3}^2}{\gamma_{R_2SO_4}} = \frac{q/q_\infty}{(1-q/q_\infty)^2} \frac{(1-C/C_o)^2}{C/C_o} \frac{C_o\mu}{\rho q_\infty} \tag{15}$$

or,

$$\frac{q/q_\infty}{(1-q/q_\infty)^2} = \overline{K} \frac{C/C_o}{(1-C/C_o)^2} \tag{16}$$

where,

$$\overline{K} = K_o \frac{\gamma_{RHCO_3}^2}{\gamma_{R_2SO_4}} \frac{\rho q_\infty}{C_o\mu} \tag{17}$$

The value of $\overline{K}$ for any exchange system determines the shape of the equilibrium isotherm.

$\overline{K} \gg 1$ favorable, near irreversible equilibrium

$\overline{K} = 1$ linear equilibrium

$\overline{K} < 1$ unfavorable equilibrium

The local equilibrium is then best described by a non-linear equilibrium isotherm such a Langmuir or Freundlich isotherm shown below.

$$q_\infty = \frac{a_1 C_o}{1 + a_2 C_o} \qquad \text{Langmuir} \tag{18}$$

$$q_\infty = A C_o^a \qquad \text{Freundlich} \tag{19}$$

Rate Controlling Mechanisms

A study of the behavior of a fixed bed ion-exchange system must include not only the effects of the ionic equilibrium on the system, but also the mechanisms which control the rate of mass transfer. There are four important mass transfer steps in an ion-exchange resin-based system.

1. Fluid-phase external mass transfer
2. Fluid-phase pore diffusion
3. Reaction at the phase boundary
4. Solid phase diffusion

Pore diffusion refers to mass transfer in the fluid film within the pores of the ion-exchange resin. This mechanism can be neglected if it is assumed that the amount of solute held by the fluid in the pores is small compared with the amount adsorbed by the resin phase. The reaction rate at the fluid-solid interface will be relatively fast mainly because the exchanging ions are strong ions [14].

If mechanisms (2) and (3) are neglected, the rate of exchange between the fluid and solid particles is then given by the combined effect of external and solid phase diffusion. For external film diffusion, the rate is given by:

$$\frac{\partial q(z,t)}{\partial t} = k_l a(C - C_s) \tag{20}$$

where k_l is the liquid side mass transfer coefficient and a is the surface area per unit volume of the particle. For solid phase diffusion, the expressions for the concentration in the resin particles will be given by:

$$\frac{\partial q_i}{\partial t} = \frac{D}{r^2}\frac{\partial}{\partial r}\left(r^2\frac{\partial q_i}{\partial r}\right) \tag{21}$$

where D is the diffusivity and q_i is the local resin phase concentration The average concentration of the particles is then given by equation (22). $q(z,t)$ presented in equation (22) is a volume averaged value of the concentration in the resin particles at time t, for bed cross section situated at height z.

$$q(z,t) = \frac{3}{R^3}\int_0^R q_i(r,z,t)r^2 dr \tag{22}$$

and the surface concentration $q_i(R,z,t)$ is described by the Langmuir type isotherm as:

$$q_i(R,z,t) = \frac{a_1 C_s}{1 + a_2 C_s} \tag{23}$$

The equilibrium and mass transfer relationships and the material balance expression given in equation (8), provide the necessary elements for the mathematical model of the ion-exchange resin-based system being studied.

Mathematical Model

The equations presented above can be simplified by a change of variables given by: $X = \frac{z}{mv}$, and $\theta = t - \frac{z}{v}$. This converts equation (8) to:

$$\frac{\partial C}{\partial X} + \frac{1}{m}\frac{\partial q}{\partial \theta} = 0 \tag{24}$$

The rate expression transforms as follows:

$$\frac{\partial q_i}{\partial \theta} = \frac{D}{r^2}\frac{\partial}{\partial r}\left(r^2 \frac{\partial q_i}{\partial r}\right) \tag{25}$$

The average concentration in the resin particles is now given by:

$$q(X,\theta) = \frac{3}{R^3}\int_0^R q_i(r,X,\theta) r^2 dr \tag{26}$$

and the resin phase surface concentration described by equation (23) becomes:

$$q_i(R, X, \theta) = \frac{a_1 C_s}{1 + a_2 C_s} \tag{27}$$

Because the above system of equations is non-linear, an exact solution cannot be obtained; however, by applying the proper initial and boundary conditions the system can be reduced to a partial-integro differential equation which can be solved by numerical methods. The initial and boundary conditions which apply to this system are listed below.

$$q(\theta = 0) = 0$$

$$C(X = 0) = C_o$$

$$\frac{\partial q_i}{\partial r}(r = 0) = 0$$

$$q_i(R, X, \theta) = \frac{a_1 C_s}{1 + a_2 C_s}$$

Solving the diffusion equation (25) gives,

$$H(r, \theta) = 1 - 2 \cdot \sum_{n=0}^{\infty} \frac{(-1)^{(n+1)}}{\frac{n\pi}{R} r} exp\left[-D\left(\frac{n\pi}{R}\right)^2 \theta sin\left(\frac{n\pi}{R}\right) r\right] \tag{28}$$

where $H(r, \theta)$ is the solution to equation (25) when the surface concentration $q_i(R, X, \theta)$ is unity. Applying Duhamel's theorem to the result given in (28) gives a convenient relationship between this solution for fixed surface concentration and the case of variable surface concentration:

$$q_i(r, X, \theta) = \int_0^{\theta} q_s(x, \lambda) \frac{\partial}{\partial \theta}(H(r, (\theta - \lambda)))d\lambda \tag{29}$$

where λ is a dummy variable of integration, and $\frac{\partial H(r,\theta)}{\partial \theta}$ is given by:

$$\frac{\partial H(r, \theta)}{\partial \theta} = 2D \cdot \sum_{n=1}^{\infty} (-1)^{(n+1)} \sigma_n \frac{sin(\sigma_n r)}{r} exp\left[-D\sigma_n^2 \theta\right] \tag{30}$$

where $\sigma_n = \frac{n\pi}{R}$. Substitution of equation (30) into (29) and interchanging the order of integration will yield:

$$q_i(r, x, \theta) = 2D \cdot \sum_{n=1}^{\infty} (-1)^{(n+1)} \sigma_n \frac{sin(\sigma_n r)}{r} \int_0^{\theta} q_s(X, \lambda) exp\left[-D\sigma_n^2 \theta - \lambda\right] d\lambda \tag{31}$$

By means of equation (26), the radial dependence of the concentration can be removed and (31) becomes:

$$q(x, \theta) = \frac{6D}{R^2} \cdot \sum_{n=1}^{\infty} \int_0^{\theta} q_s(X, \lambda) exp\left(-D\sigma_n^2 (\theta - \lambda)\right) d\lambda \tag{32}$$

Differentiation of equation (32) with respect to theta will give the following expression for the rate of uptake by the resin phase:

$$\frac{\partial q}{\partial \theta} = \frac{6D}{R^2} \cdot \sum_{n=1}^{\infty} \int_0^{\theta} q_s(X, \lambda) exp\left(-D\sigma_n^2 (\theta - \lambda)\right) d\lambda \tag{33}$$

Finally, applying the material balance condition of equation (24) yields:

$$\frac{\partial C}{\partial X} = -\frac{6Da_1}{mR^2} \cdot \sum_{n=1}^{\infty} \int_0^{\theta} \frac{\partial (C/(1+a_2C))}{\partial \lambda} exp\left(-D\sigma_n^2(\theta - \lambda)\right) d\lambda \qquad (34)$$

The expression can be generalized if the concentration variable is made dimensionless. If $\phi = \frac{C}{C_o}$ then (34) becomes:

$$\frac{\partial \phi}{\partial X^*} = -2 \cdot \sum_{n=1}^{\infty} \int_0^{\theta^*} \frac{\partial (\phi/(1+a_3\phi))}{\partial \lambda} exp\left(-\frac{1}{2}n^2\pi^2(\theta^* - \lambda)\right) d\lambda \qquad (35)$$

where,

$$X^* = \frac{3Da_1X}{mR^2} = \frac{3Da_1z}{mR^2v}$$
$$\theta^* = \frac{2D}{R^2}(t - \frac{z}{v})$$
$$a_3 = a_2C_o$$

The partial-integro differential equation (35) derived in this section is the starting point for the numerical solution to the system of equations developed by Antonson. The boundary conditions for this equation are $\phi(X^* = 0) = 1$, $q_i(\theta^* = 0) = 0$ and the initial condition is $\phi(\theta^* = 0) = 0$. The details of Antonson's formulation of the numerical solution to this equation and the computer code he developed are presented in Appendix A.

CHAPTER IV

EXPERIMENTAL EQUIPMENT AND PROCEDURE

The objective of the experimental program was to determine the effects of temperature, pressure, flowrate, concentration and bed height on the behavior of a sulfate bicarbonate ion-exchange system where carbonation and exhaustion steps are carried out simultaneously. This was accomplished by carrying out a series of fixed bed experiments to obtain breakthrough curve data. The equipment and procedures used in performing these experiments will be discussed in the following sections.

Apparatus

A schematic diagram of the experimental apparatus is shown in Figure 7. It included a fixed bed consisting of a thick-walled Pyrex glass column, a rotameter, a pressure gauge and a liquid reservoir. The column was equipped with two inlets: one for the fluid and the other for the CO_2 gas. The resin bed was supported by a fine wire screen. The fluid was fed to the column from a heated reservoir, and the flow rate through the column was controlled at the column outlet. The pressure in the column was measured by a pressure gauge mounted at the column inlet. Rohm & Haas supplied Amberlite IRA-68 was the ion-exchange resin used in this study. A summary of the physical properties of this anion-exchange resin is given in Table I. Carbon dioxide used for the carbonation of the resin was 99.99% pure.

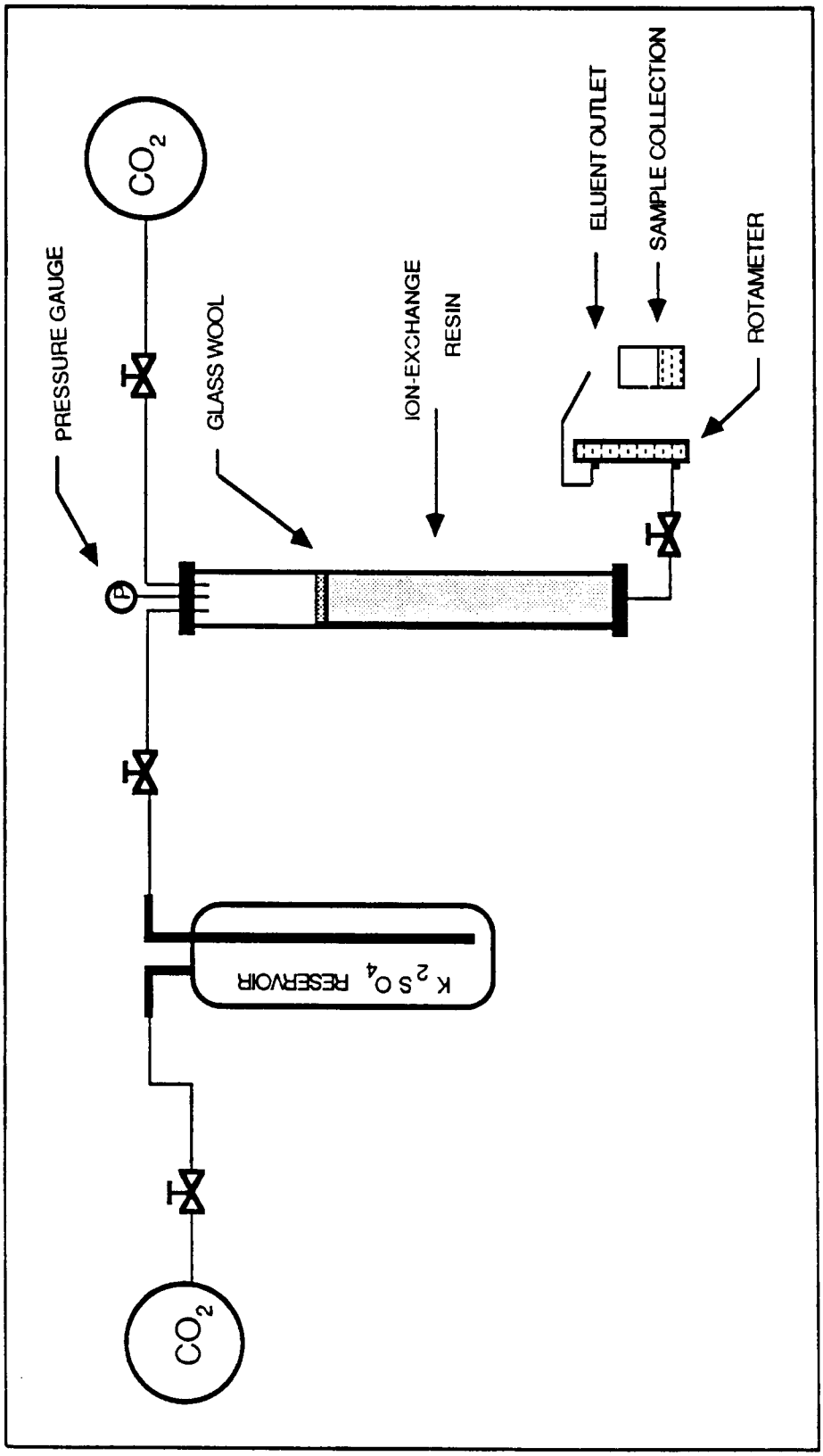


Figure 7. Schematic diagram of experimental apparatus

Table I.

Physical Characteristics of Amberlite IRA-68 [15]

Ionic form	Free base OH^-
Moisture Content	60%
Effective Particle Diameter	.45mm.
Screen Grading	(.3 - 1.2)mm. U.S. Mesh 16-20
Total Exchange Capacity	1.6 meq/ml as $CaCO_3$
Particle Density	$720 gms/l$

Experimental Procedure

In order to carry out the experiments in the fixed bed, the column was filled with deionized water and the resin particles were dropped into the water to allow for a random packing of the bed. After the column was packed to the desired bed height, it was placed under CO_2 pressure in order to initiate the reaction between the hydroxide ions on the active sites of the resin and the CO_2 gas. This reaction would then result in the formation of bicarbonate ions on the active sites of the resin. It must be noted that during this reaction, the level of water in the column was the same as that of the resin in the column. This step in the process lasted for about five minutes prior to the introduction of potassium sulfate into the column. After the potassium sulfate had been introduced into the column, samples of the effluent were taken at various time intervals after the known volume of water which was in the column had been withdrawn. A fresh batch of resin was used for each run, therefore, it was not necessary to regenerate any of the resin previously exhausted. Analysis of the effluent samples for sulfate ion concentration was carried out using the Dionex Ion Chromatograph.

To verify the reproducibility of the data, two of the experimental runs were repeated using fresh batches of resin. Results from these runs, given in Figures 8 and 9 show good reproducibility. In addition to this reproducibility check, an experimental run was carried out at conditions close to those of Butler in an attempt to reproduce his data. The breakthrough curve obtained from this run compared well with the one obtained by Butler at similar conditions. The conditions used for this reproducibility check were C_o = 50000 ppm, T = $20°C$, Flow rate = 10 cc/min, and bed height = 18 ins. The run was also done under a CO_2 pressure of 5 psig while Butler's was at 0 psig. The curve obtained from this run is shown in Figure 10.

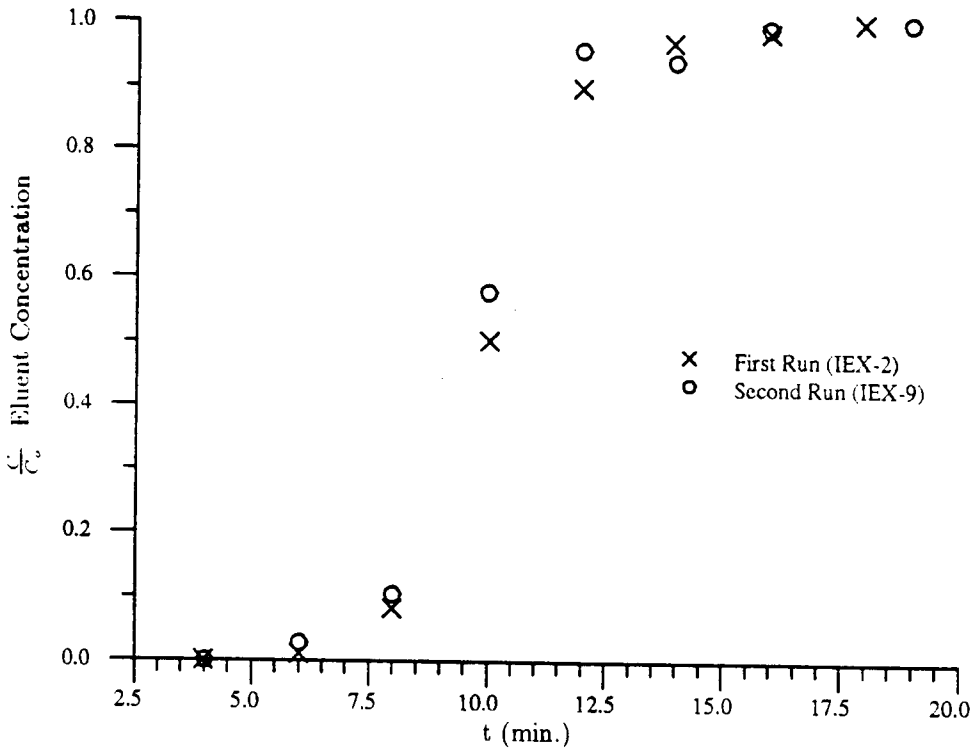


Figure 8. Reproducibility check of Run IEX-2

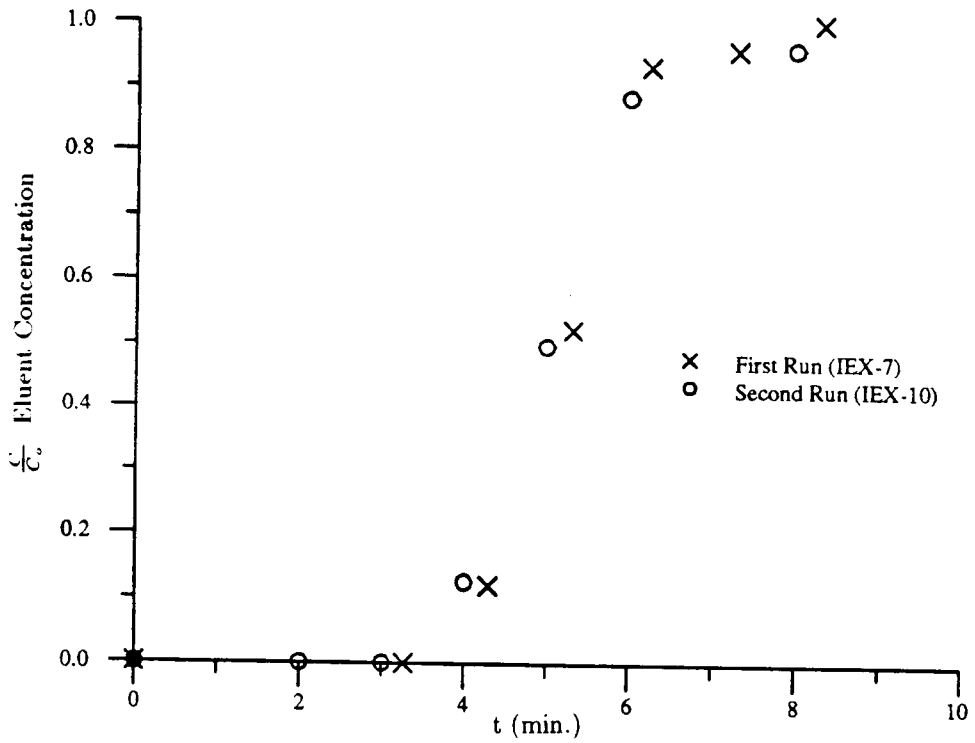


Figure 9. Reproducibility check of Run IEX-7

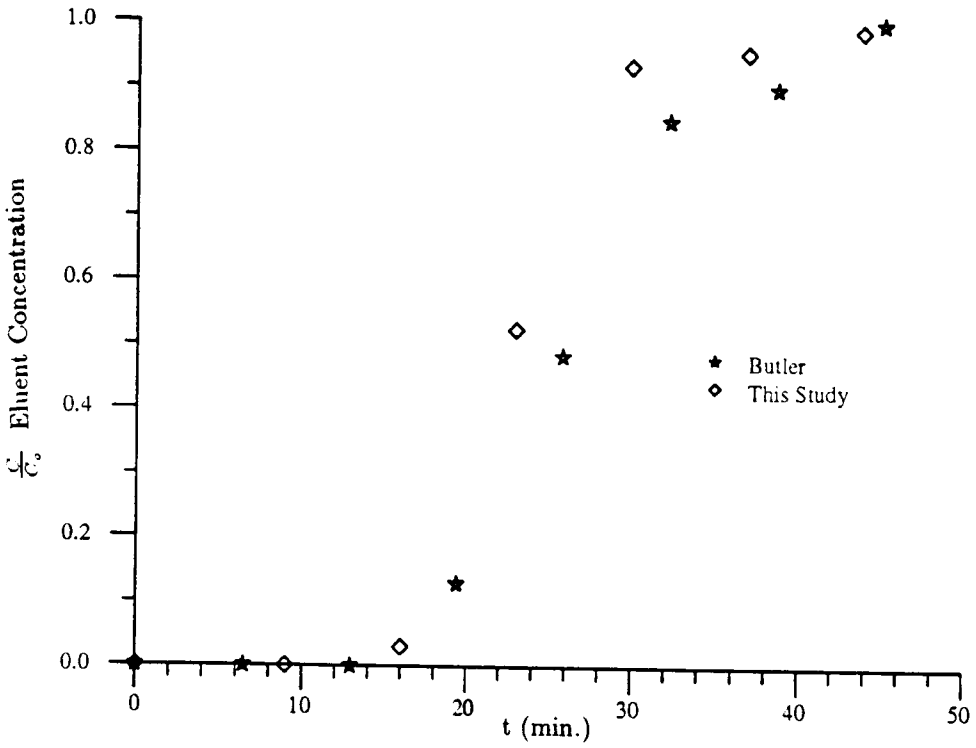


Figure 10. Reproducibility check of Butler's Data

CHAPTER V

RESULTS AND DATA EVALUATION

The experimental data and results obtained from the analysis of fixed bed experiments will be presented in this section. In order to get the experimental data, a series of fixed bed runs were carried out at various conditions of pressure, temperature, flowrate, bed height, and concentration. Table II presents a summary of the experimental conditions used in each run.

Experimental Breakthrough Curves

Data from the fixed bed experiments gave information about the concentration of sulfate remaining in a solution of potassium sulfate which passed through a bed of ion-exchange resin as a function of time. These data were plotted as $\frac{C}{C_o}$ vs. t where, C_o is the initial concentration and t is time. Figures 11 and 12 show semi-log plots of $\frac{C}{C_o}$ vs. t. The curves shown in Figure 11 describe breakthrough data at conditions IEX-1 through IEX-4 as described in Table II. Curves shown in Figure 12 describe breakthrough data for conditions IEX-5 through IEX-8. The validity of the mathematical model used was checked by comparing the experimental curves to theoretical curves with similar values of a_2C_o . This curve matching technique will be discussed further in the subsequent sections.

Table II.
Conditions used for fixed bed experiments

Run	Inlet K_2SO_4 $Conc.C_o(ppm)$	Column CO_2 Pressure P (psig.)	Column Temp. T (^oC)	Solution flow rate V (cc/min)	Bed Height z (ins.)
IEX-0	50000	5	20	10	18
IEX-1	8000	20	20	50	9
IEX-2	30000	20	20	50	9
IEX-3	70000	20	20	50	9
IEX-4	100000	20	20	50	9
IEX-5	8000	40	65	120	18
IEX-6	30000	40	65	120	18
IEX-7	70000	40	65	120	18
IEX-8	100000	40	65	120	18
IEX-9	30000	20	20	50	9
IEX-10	70000	40	65	120	18

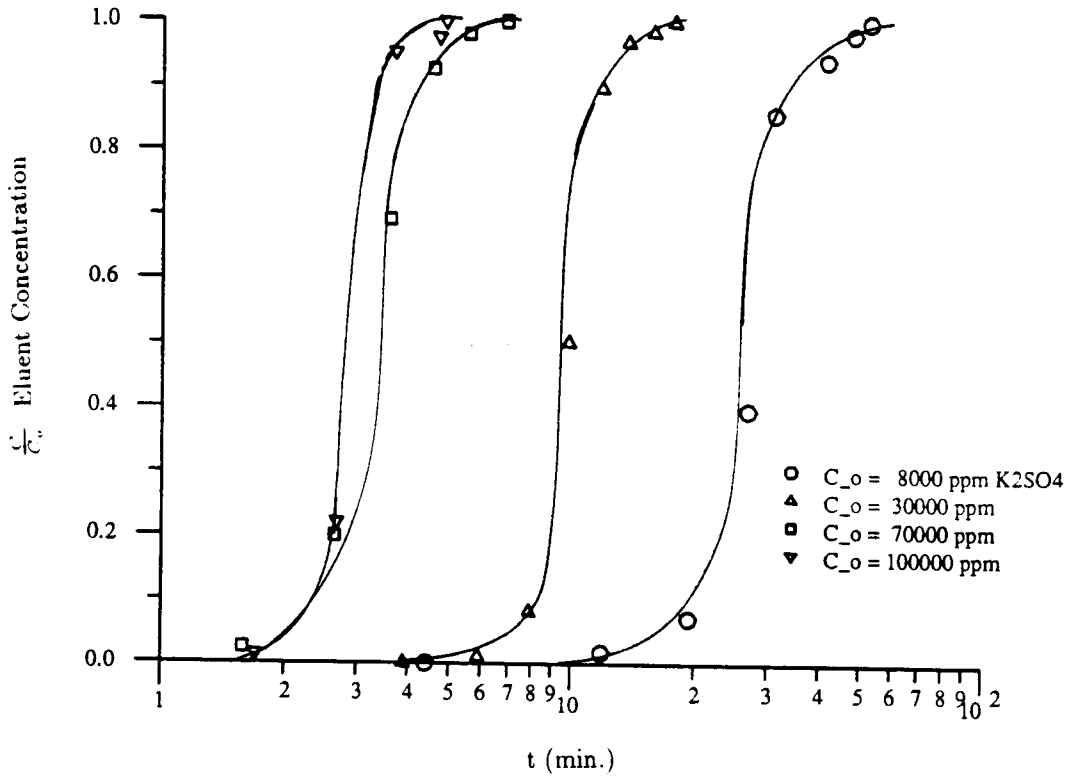


Figure 11. Experimental breakthrough curves for runs IEX-1 - IEX-4

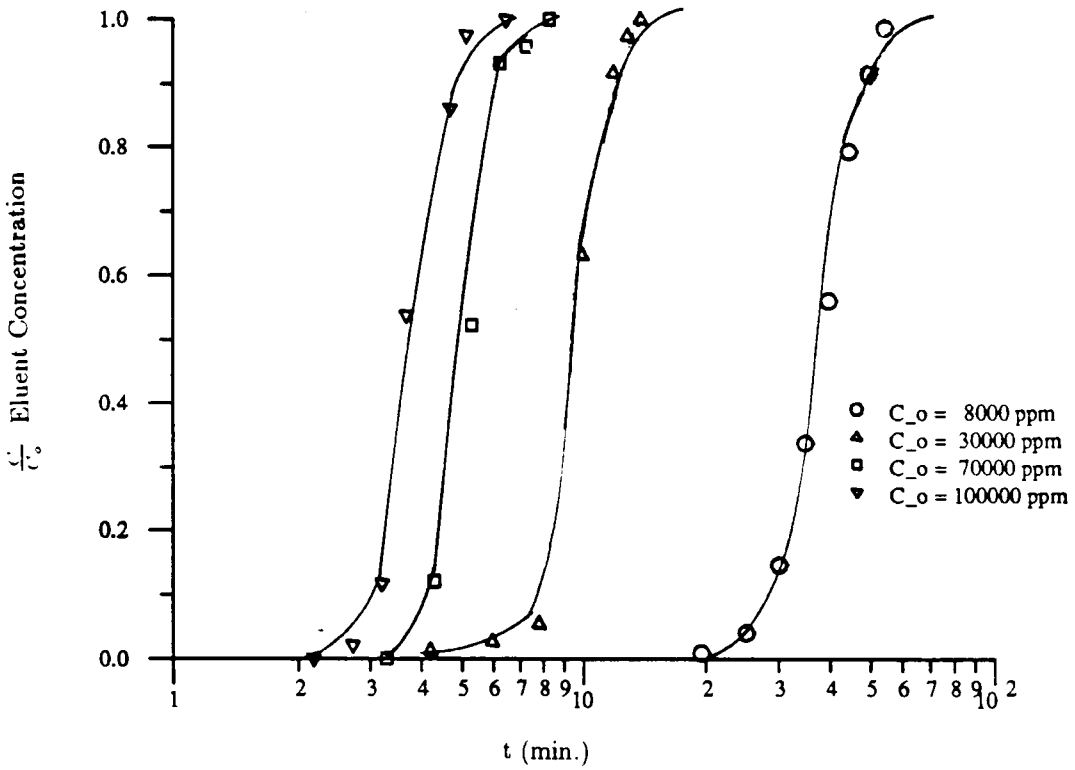


Figure 12. Experimental breakthrough curves for runs IEX-5 – IEX-8

Determination of Equilibrium Capacity

One of the objectives of these experiments was to determine the equilibrium capacity of the resin for a specific set of experimental conditions. This information can be obtained from the breakthrough data, and is based upon a material balance done around the fixed bed.

$$VC_o - VC = V_R \frac{dq}{dt} \tag{36}$$

where V_R is the volume of the resin in the bed, V is the volumetric flowrate, C_o is the bulk concentration of the adsorbate at the inlet, C is the outlet concentration of adsorbate, and q is the average concentration of adsorbate in the resin phase. Equation (36) can be rearranged to give:

$$V(C_o - C) = V_R \frac{dq}{dt} \tag{37}$$

$$VC_o(1 - \frac{C}{C_o}) = V_R \frac{dq}{dt} \tag{38}$$

Separation of variables and integration would yield:

$$VC_o \int_0^{t_\infty} (1 - \frac{C}{C_o}) dt = V_R \int_0^{q_\infty} dq \tag{39}$$

where t_∞ is the time at $\frac{C}{C_o} = 1$, and q_∞ is the equilibrium capacity of the resin. Equation (39) suggests that the area under a plot of $(1 - \frac{C}{C_o})$ vs. t would yield the equilibrium capacity when multiplied by a factor of $\frac{VC_o}{V_R}$. Figure 13 shows a

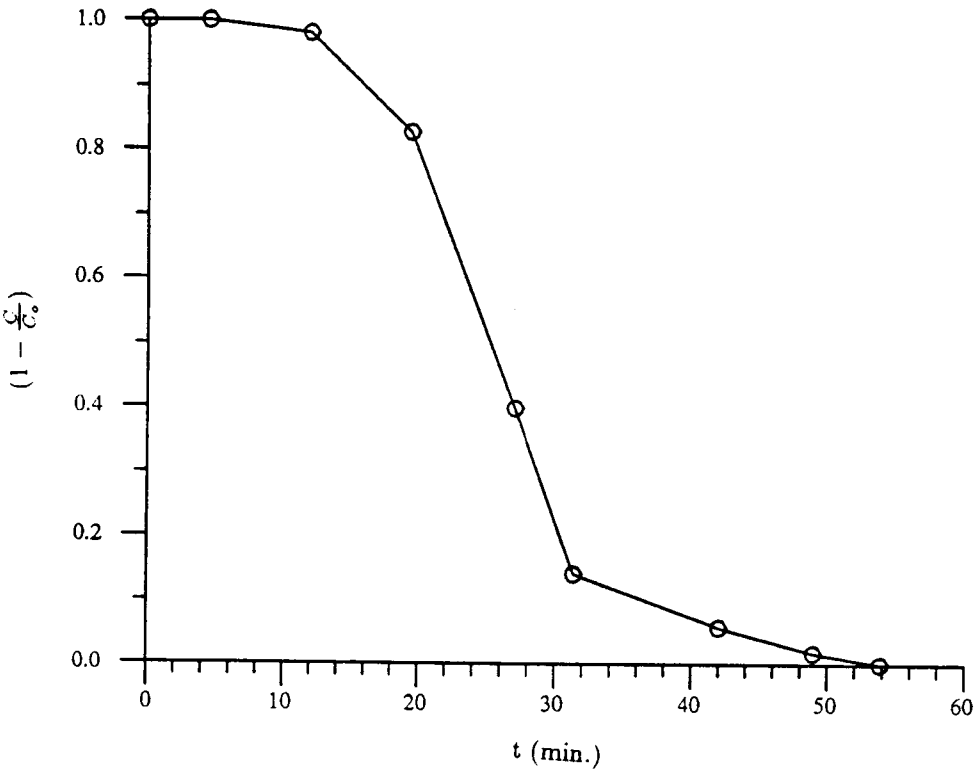


Figure 13. Plot of $(1 - \frac{C}{C_o})$ vs. t for run IEX-1

plot of $(1-\frac{C}{C_o})$ vs. t for run IEX-1. The area in these calculations was determined graphically using a FORTRAN program based on the method of trapezoids. This program is given in Appendix A.

Determination of Equilibrium Isotherm

The equilibrium resin capacity q_∞ is related to the inlet concentration C_o by the Langmuir equilibrium isotherm:

$$q_\infty = \frac{a_1 C_o}{1 + a_2 C_o} \tag{18}$$

With the equilibrium resin capacity q_∞ obtained from the material balance on the column, an attempt can be made to obtain the constants a_1 and a_2 using regression techniques. To accomplish this task, equation (18) was linearized and the following expression was obtained:

$$\frac{C_o}{q_\infty} = \frac{1}{a_1} + \frac{a_2}{a_1} C_o \tag{40}$$

The plot of $\frac{C_o}{q_\infty}$ vs. C_o shown in Figure 14 is linear with a slope of $\frac{a_2}{a_1}$ and intercept value of $\frac{1}{a_1}$. The values of q_∞ and C_o used for this regression are presented in Table III. The equilibrium isotherms, shown in Figure 15, were calculated from regressed values of a_1 and a_2 and compared favorably with the experimental data. Further examination of these curves show that beyond C_o value of about 0.015 the equilibrium capacity becomes constant and remains a function of pressure only. Table IV gives the values of a_1 and a_2 obtained from the regression analysis of the equilibrium data.

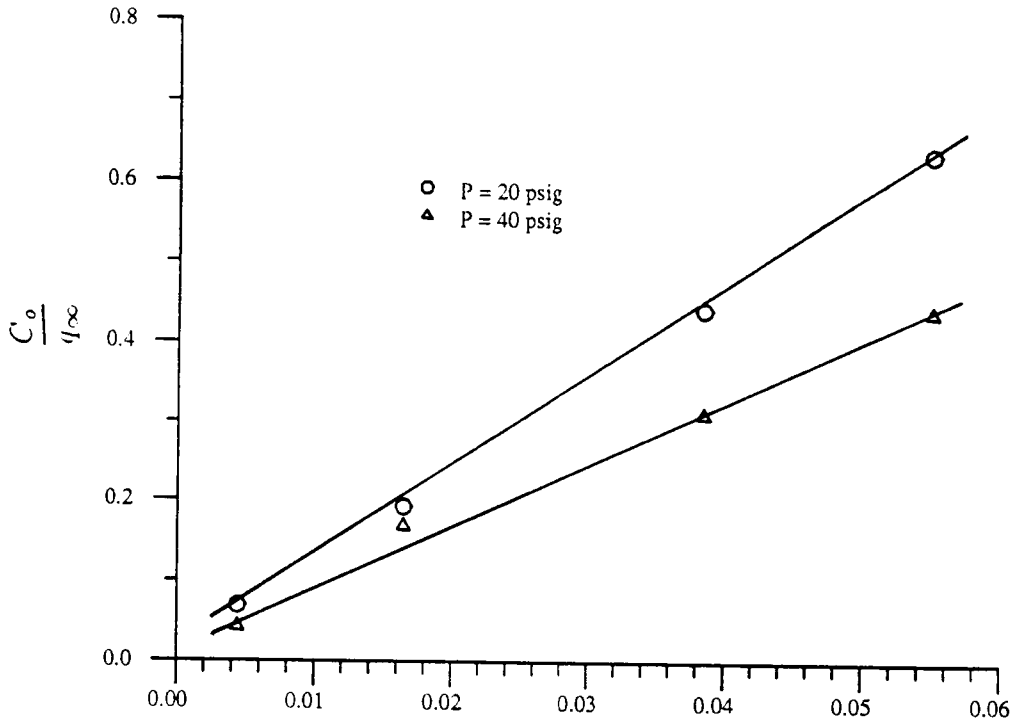


Figure 14. Fit of linearized Langmuir isotherm to experimental data

Table III.

Data used for Equilibrium Isotherm Calculations

$C_o \frac{gms.SO_4^{2-}}{ml}$	$q_\infty \frac{gms.SO_4^{2-}}{ml.resin}$		$\frac{C_o}{q_\infty}$	
	$P = 20psig.$	$P = 40psig.$	$P = 20psig.$	$P = 40psig.$
.004	.059	.103	.068	.043
.016	.086	.097	.191	.168
.038	.087	.124	.441	.310
.055	.087	.126	.633	.437

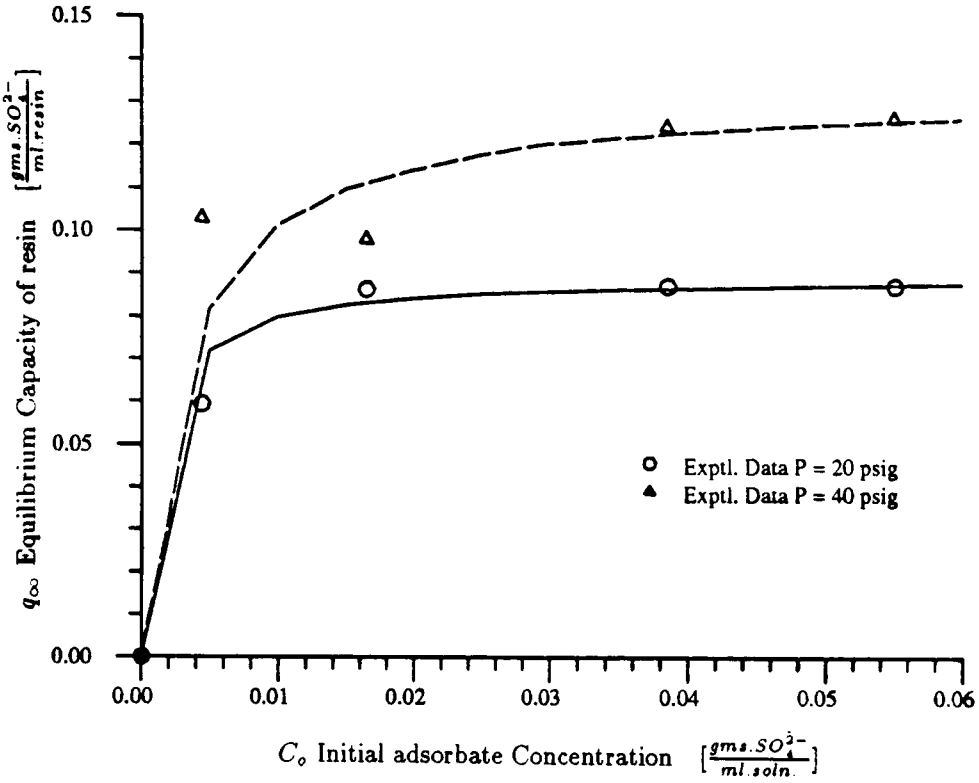


Figure 15. Comparison of equilibrium isothems with experimental data

Table IV.

Langmuir Constants

a_1†		a_2	$[\frac{ml resin}{gm}]$
P = 20 psig	P = 40 psig	P = 20 psig	P = 40 psig
74.07	42.73	830.2	322.2

† dimensionless

Determination of Diffusion Coefficients

The determination of the diffusion coefficients begins first with plotting the experimental breakthrough data as a semi-log plot of $\frac{C}{C_o}$ vs. θ and then comparing it to a similar semi-log theoretical plot of $\frac{C}{C_o}$ vs. θ^*, where θ^* is given by $\theta^* = \frac{2D}{R^2}(t - \frac{z}{v})$ and $\theta = (t - \frac{z}{v})$. The use of semi-log plots in the curve matching process is done in order to make the relationship between θ and θ^* just a displacement along the x-axis [27]. This relationship is given by:

$$log(\theta^*) = log(\theta) + log\left(\frac{2D}{R^2}\right) \tag{41}$$

The theoretical breakthrough curves were generated using the program developed by Antonson [9]. The most important input parameters to the computer program are the dimensionless column length X^* and equilibrium parameter a_2C_o. The parameter a_2C_o obtained from the experimental data is used to generate a set of theoretical curve at various values of X^*. The X^* value obtained from the theoretical curve which best matches the experimental breakthrough curve is then used to determine the diffusion coefficient. The value of D for the best matching curve is then obtained from the following expression:

$$X^* = \frac{3Da_1z}{mR^2v} \tag{42}$$

where a_1 is the first Langmuir constant, z is the height of the resin bed, v is the linear velocity through the bed, and m is the ratio of void fraction to particle fraction in the packed bed. The diffusion coefficient is presented as the ratio $\frac{D}{R^2}$

where R is the characteristic length of the resin particle and D is the effective diffusion coefficient. This method of presenting the diffusion coefficient is used to facilitate comparison with values obtained by other researchers who also presented their data in this form, and also because the occurence of micropore or macropore diffusion is related to the characteristic length (R) of the resin phase. Table V presents the diffusion coefficients obtained from the best fit of the experimental breakthrough curves. Figure 16 shows a set of theoretical curves obtained using Antonson's model. The value of the parameter $a_2 C_o$ used is 1.42, and X^* values used ranged from 0.9 to 2.5 .

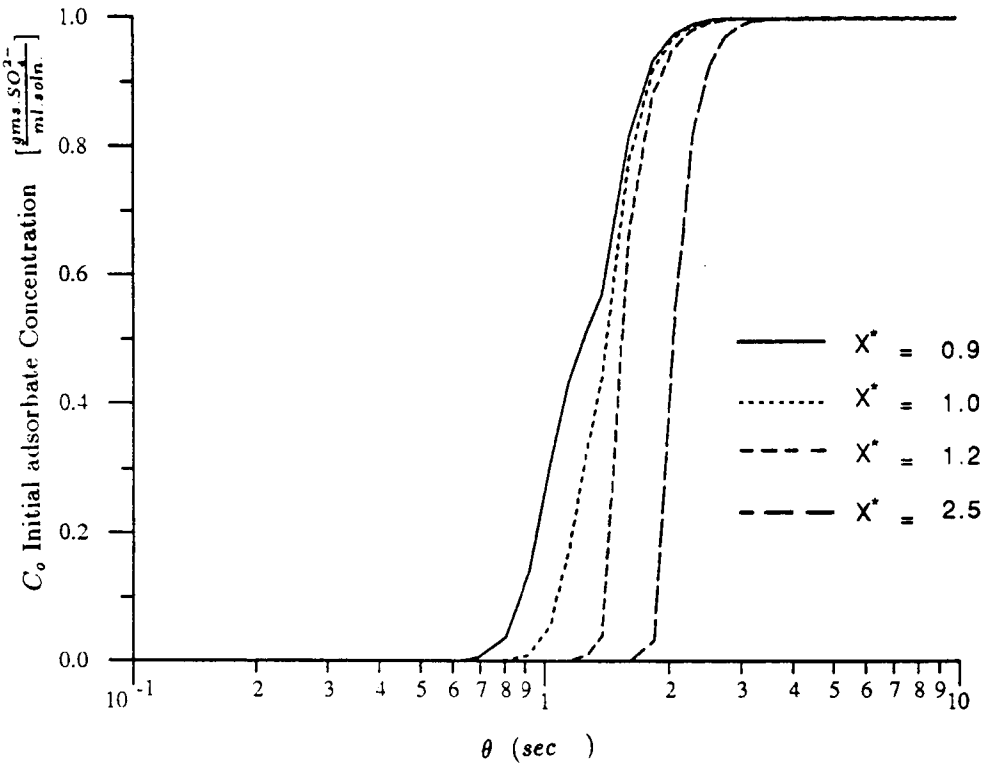


Figure 16. Theoretical breakthrough curves obtained from Antonson's model

Table V.

Diffusion Coefficients from Best Fit of Experimental Breakthrough Curves

C_o	X^*	$\frac{D}{R^2}\ sec^{-1}$	
		$P = 20psig.$	$P = 40psig.$
.004	3.31	0.050×10^{-3}	—
.016	12.00	0.183×10^{-3}	—
.038	28.00	0.428×10^{-3}	—
.055	40.00	0.60×10^{-3}	—
.004	0.95	—	$.030 \times 10^{-3}$
.016	4.80	—	0.152×10^{-3}
.038	11.0	—	0.350×10^{-3}
.055	16.00	—	0.509×10^{-3}

CHAPTER VI

DISCUSSION OF RESULTS

The results obtained from the fixed bed experiments and presented in the previous chapter will be discussed further in this section. The main goal of the discussion will be to provide an interpretation of the experimental results. The major points to be discussed in this section are: (1) The experimental equilibrium data, (2) The diffusion coefficients obtained from the analysis of the breakthrough curves, and (3) The compatibility of the mathematical model with the experimental data.

Equilibrium Data

The equilibrium data obtained from the fixed bed experiments are very important, because they can serve as major design parameters for an ion-exchange resin-based seed regeneration plant. The system parameters which were used in the fixed bed experiments were varied in order to determine the effect of each one on the equilibrium capacity of the resin. Results from the fixed bed runs showed that the equilibrium capacity varied noticeably with changes in the inlet concentration of the adsorbate and approached a limiting value at high values of the inlet concentration. This result is in line with the assumption of the Langmuir type equilibrium isotherm applied in this study. Examination of the values of a_1 and a_2 obtained from the experimental breakthrough data shows that the equilibrium of the exchange system is non-linear. Vermeulen, *et. al.* [22], gave a similar expression for the Langmuir isotherm which is given by equation (43).

$$q_\infty = \frac{QKC_o}{1 + KC_o} \tag{43}$$

where Q is the maximum asymptotic solid phase concentration in the resin phase and K is the equilibrium constant as defined by Vermuellen. Comparing equation (43) with equation (18), it is evident that $a_1 = QK$ and $a_2 = K$. For the sulfate-bicarbonate ion-exchange system, the equilibrium constant defined by Butler is given by:

$$\overline{K} = K_o \frac{\gamma^2_{RHCO_3} \rho q_\infty}{\gamma_{R_2SO_4} C_o \mu} \tag{6}$$

Figure 6 shows that for values of $\overline{K}$ much greater than 1, the equilibrium of the exchange reaction becomes more non-linear. Since K and $\overline{K}$ are the same, and the values obtained for a_2, at 20 and 40 psig respectively (830, and 322) are much greater than one, it can be said that the sulfate-bicarbonate system is non-linear.

An upward trend in the equilibrium capacity of the resin was observed with an increase in the CO_2 pressure. This trend is maintained when the experimental data are compared with data obtained by Butler [1] from his fixed bed experiments at atmospheric pressure and in the absence of CO_2 atmosphere. Figure 17 shows plots of the equilibrium isotherms as a function of concentration with CO_2 pressure as a parameter. The increase in the resin-capacity is attributed to the increase in CO_2 pressure because, as the CO_2 pressure is increased, the resin carbonation reaction (1):

$$CO_2 + ROH \longrightarrow RHCO_3 \tag{1}$$

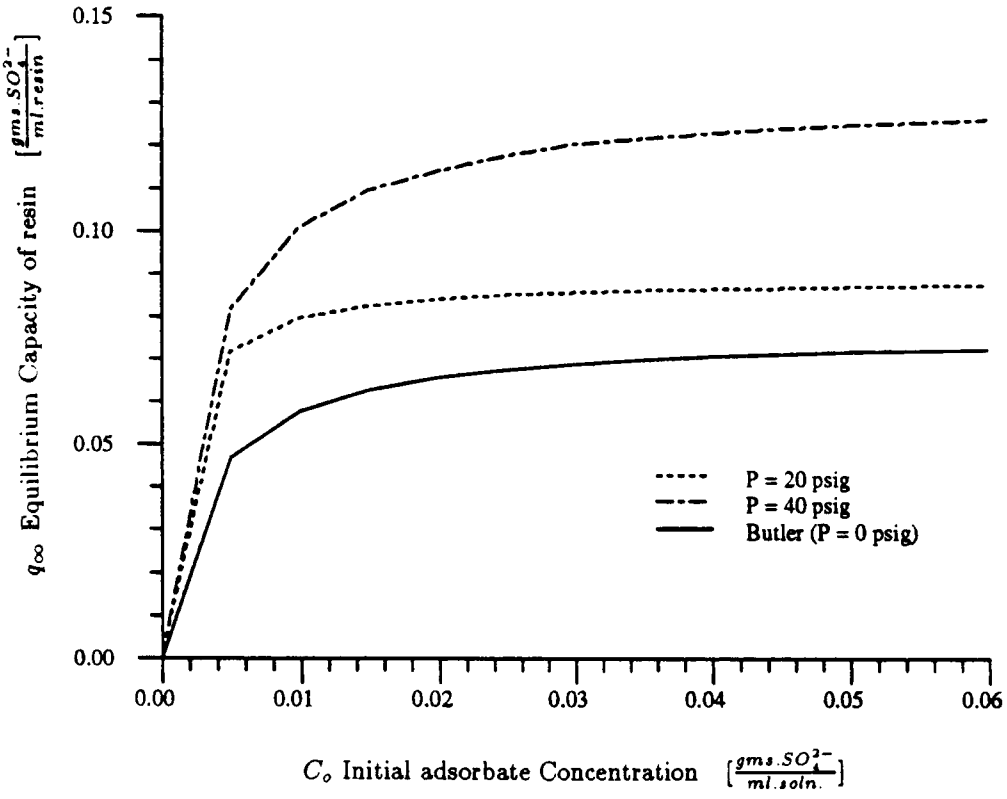


Figure 17. Comparison of equilibrium isotherms at various CO_2 pressures

would shift to the right and favor production of bicarbonate at the active resin sites. Furthermore, placing the system under CO_2 pressure prevents any bicarbonate on the resin from decomposing to the carbonate form which is found to be detrimental to the uptake of sulfate ions. This decomposition reaction is given by equation (44). Thus with more bicarbonate ions available on the active sites, and a higher resin affinity for sulfate ions than bicarbonate ions, the increase in capacity is a reasonable effect.

$$R_2CO_3 + CO_2 + H_2O \longrightarrow 2RHCO_3 \tag{44}$$

Diffusion Coefficients

The diffusion coefficients obtained from the fixed bed runs were determined by using the curve matching technique described in Chapter V. From the values for $\frac{D}{R^2}$ in Table V it is evident that as the inlet concentration of the adsorbate species increased, the ratio $\frac{D}{R^2}$ also increased. The increase in these values could be attributed to an increase in the driving force for mass transfer due to the change in concentration and suggests that a diffusion mechanism such as micropore diffusion or macropore diffusion could be the dominant mass transfer mechanism. Liberti and Passino's [18] study of the SO_4^{2-}/Cl^- exchange system gave results which suggested that concentration variations in fixed bed operations with weak base resins, such as Amberlite IRA-68, would affect the rate of the chemical exchange reaction and the rate of diffusion into the resin.

The effect of superficial velocity on the liquid-side diffusion was considered to be negligible for the sulfate-bicarbonate system based on data presented by Butler [1] which showed that for superficial velocities above $1.2\frac{cm}{min.}$ the film side mass transfer coefficient $k_l a$ approached a constant value of $0.65\frac{cm^3}{min.gm}$. Furthermore,

the mathematical model which he applied to the system assumed that only liquid-side diffusion was controlling. As a result, it failed to predict the breakthrough behavior in the region where $\frac{C}{C_o}$ was greater than 0.8 and particle-side diffusion was indicated as a possible rate controlling mechanism. Since the superficial velocities used in this study were higher $(6.99, 16.8)\frac{cm}{min}$ than those used by Butler for the sulfate-bicarbonate system, based on his results, there should be no change in the value of the liquid-side mass transfer coefficient at these values.

The $\frac{D}{R^2}$ values obtained in this study were compared to those obtained by other researchers in order to see if the results were comparable. These comparisons were made for the work of Sheth [27] who investigated the adsorption of Ethylene on Linde 4A molecular sieves, and Ruthven [25], who investigated the adsorption of Ethane on 5A molecular sieves. The results of this comparison, given in Table VI, show that the $\frac{D}{R^2}$ values obtained in this study were in the same range as those obtained by other researchers.

Mathematical Model

The mathematical model applied in this study utilizes a particle side diffusion mechanism with a Langmuir type equilibrium to describe the ion-exchange behavior of the sulfate-bicarbonate system. Analysis of the experimental breakthrough curves of the sulfate-bicarbonate system yielded information about the equilibrium and kinetics of the system. By comparing the pertinent experimental and theoretical parameters, the mathematical model was tested for compatibility with the experimental data. The first of these tests was an attempt to find a theoretical curve which would match the experimental data. This was done using the curve matching technique described in the previous section. The values obtained for the experimental a_2C_o parameters ranged from 1.4 to 46 and theoretical

Table VI.

Comparison of Diffusion Coefficients with Literature Values

a_2C_o	T (^oC)	X^*	$\frac{D}{R^2} \times 10^3$ (sec^{-1})
.807*	24	0.6	0.092
.334*	50	0.45	0.467
.187*	75	0.55	0.86
.015**	30	7.5	1.55
.010**	40	7.5	2.56
.026**	75	11.7	5.25
3.66***	20	3.31	0.050
1.42***	65	.95	0.030
17.76***	65	16	0.509

* fixed bed Adsorption of ethylene on Linde 4A molecular sieves (Sheth [25]).
** fixed bed Adsorption of ethane on Linde 5A molecular sieves (Ruthven and Garg [27])
*** Ion-exchange of sulfate and bicarbonate on Amberlite IRA-68 (This Study)

curves generated using these values were then matched to the corresponding experimental curves.

Application of Antonson's model to the sulfate-bicarbonate system yielded theoretical breakthrough curves which compared favorably with the curves obtained experimentally. For four of the experimental runs generated in this work, Figures 18 - 21 show comparisons of the experimental and theoretical curves. The curves matched fairly well except for the portion of the curve where $\frac{C}{C_o}$ was less than 0.1. The discrepancy between the experimental and theoretical curves in this region could be attributed to the effect of liquid-side mass transfer or reaction rate control at the start of the ion-exchange process. Since neither of these mechanisms were accounted for in Antonson's model, their possible effects on the system would not show up in the theoretical breakthrough curve generated. Although Antonson's model did a fairly good job of predicting the breakthrough curves for the system, it is possible that in the earlier stage, the actual ion-exchange reaction may be governed by different kinetics than that assumed by Antonson's model. The idea of the exchange reaction being the rate controlling mechanism was considered by Liberti and Passino, who investigated the behaviour of the sulfate-chloride exchange system. While Antonson's model assumes a diffusion control mechanism, it is quite possible that the exchange reaction might be more significant to the kinetics of the system than was originally assumed. In this case, the exchange reaction involves a strongly basic divalent ion (SO_4^{2-}) and a weakly basic monovalent ion (HCO_3^-). Because the concentrations of potassium sulfate used were fairly high (8000 - 100000)ppm, the electroselectivity effect defined by Bonhoeffer *et. al.* [19] becomes less pronounced. In effect, as the aqueous phase concentration decreases, the SO_4^{2-} ions are attracted to the active resin sites with a force that is proportional to their charge density. At higher inlet

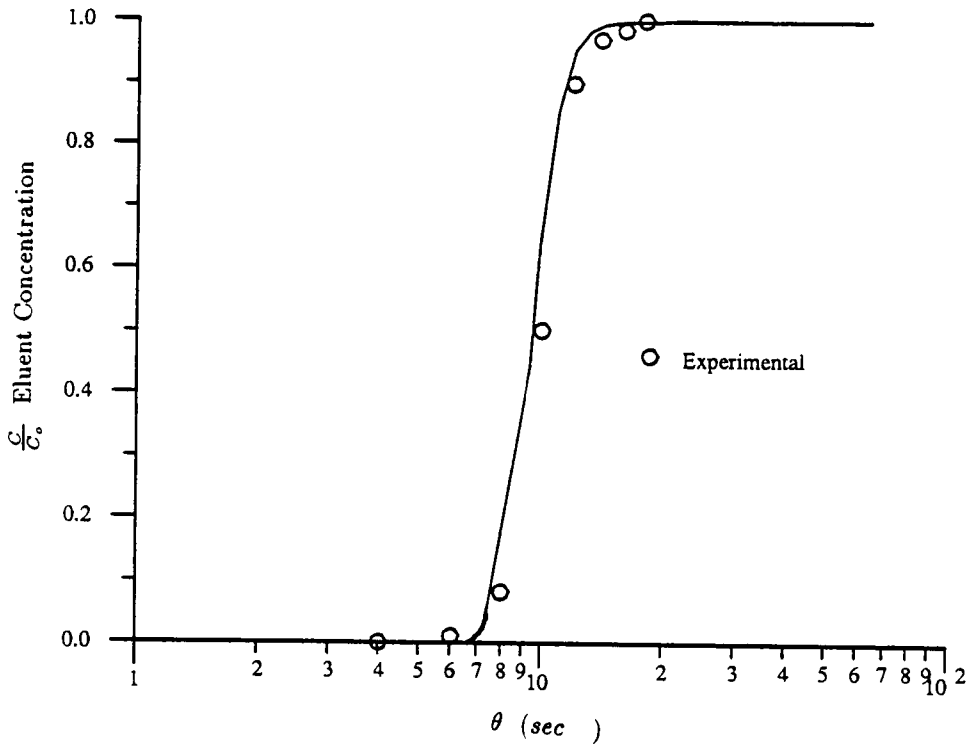


Figure 18. Match of experimental and theoretical breakthrough curves for run IEX-2: Match at $a_2C_o = 13.72$, $X^* = 12.00$.

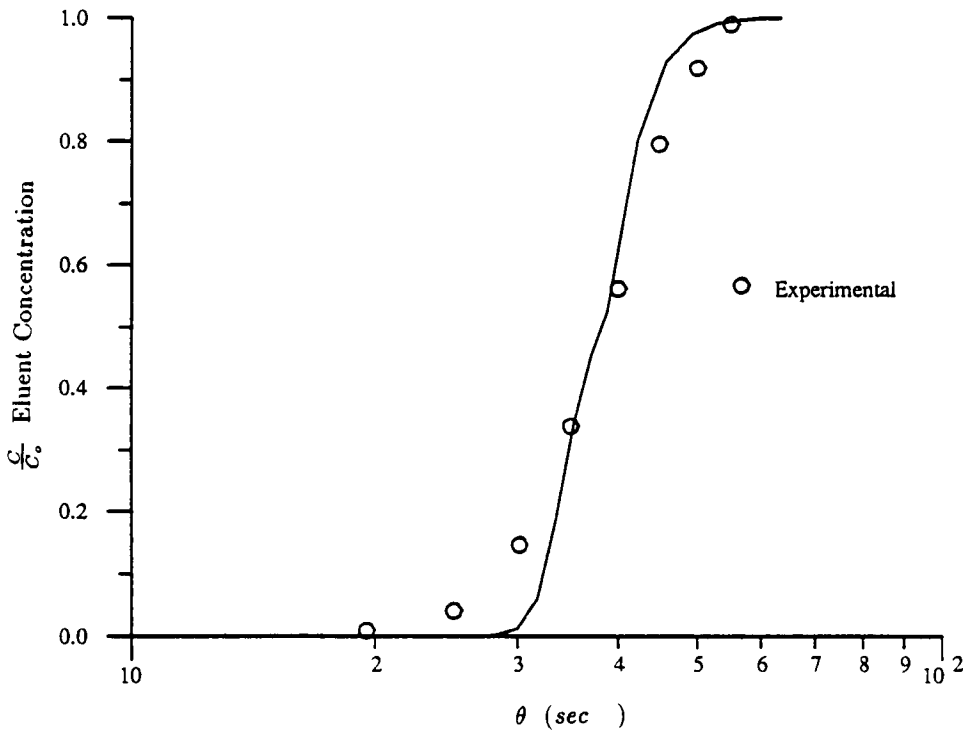


Figure 19. Match of experimental and theoretical breakthrough curves for run IEX-5: Match at $a_2C_o = 1.42$, $X^* = 0.95$ ID

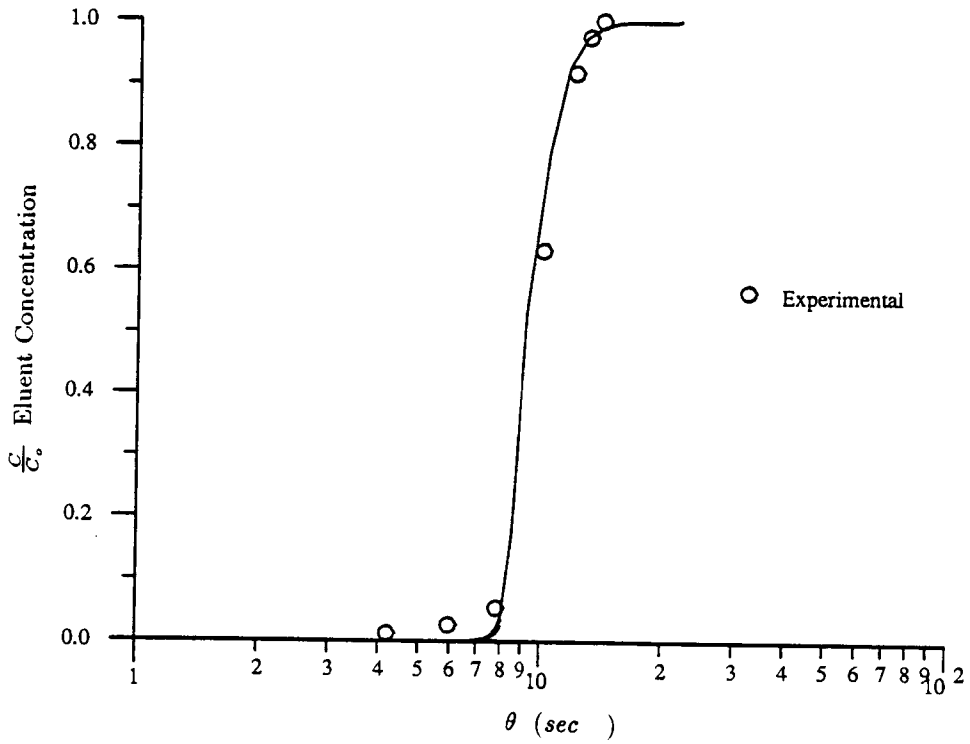


Figure 20. Match of experimental and theoretical breakthrough curves for run IEX-6: Match at a_2C_o = 5.32, X^* =4.8 +.8

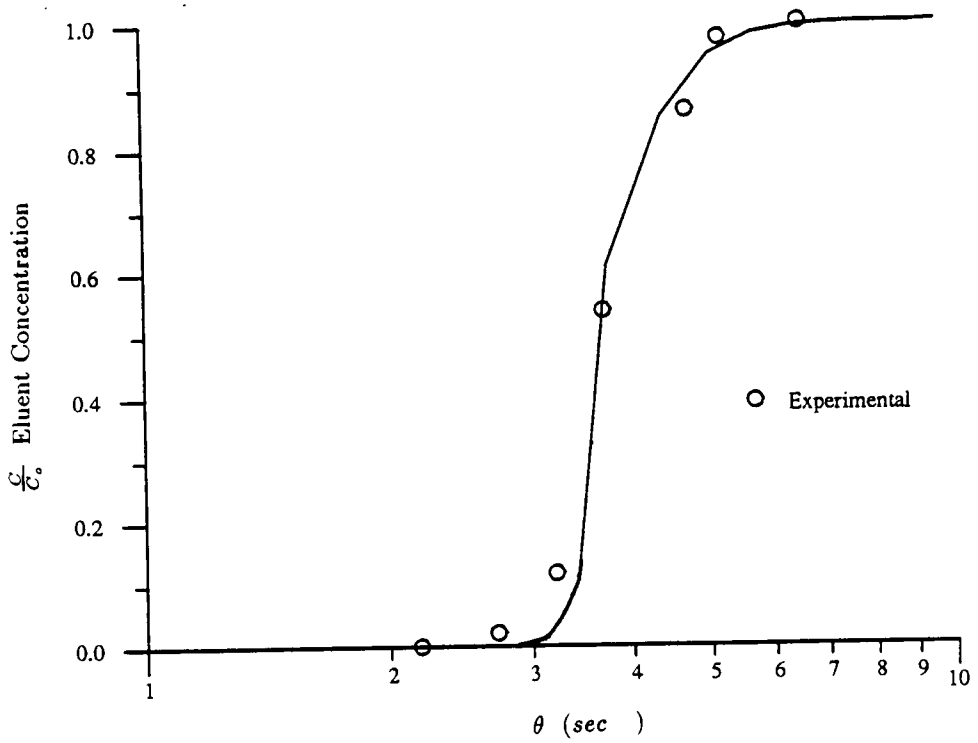


Figure 21. Match of experimental and theoretical breakthrough curves for run IEX-8: Match at $a_2C_o = 17.76$, $X^* = 16.00$

concentrations of the adsorbate, this effect would be seen to a lesser extent, thereby passing in the eluent more SO_4^{2-} ions and affecting the ultimate shape of the breakthrough curve. Application of the diffusion model of Antonson has worked fairly well in describing the behavior of the sulfate-bicarbonate system; however, the work of other researchers [18], suggest that especially in the earlier stage, the exchange reaction may have a greater role in the kinetics of the system than originally assumed.

CHAPTER VII

PROCESS DESIGN AND ECONOMICS

The results obtained from the fixed bed experiments were used in designing a full scale ion-exchange resin-based seed regeneration plant. This design was based on the results of material balance calculations performed by Resources Conservation Company (RCC) of Bellevue Washington for a MHD plant capable of producing 1000 Megawatts of electricity [23]. Table VII presents the design basis used for the material balance calculations. In addition, a preliminary economic evaluation of the process was also carried out by RCC to determine the costs associated with constructing a stand alone seed regeneration plant. A process schematic of the proposed seed regeneration plant is shown in Figure 22.

Material Balance

The assumption of pure K_2SO_4 being fed fails to take into account the fact that the flyash type material being fed to the seed regeneration plant is a multi-component mixture. Some of the other components include insoluble metal-oxides and compounds containing F^- and Cl^- ions. The fluoride and chloride ions in an actual spent seed solution could compete with sulfate ions for the active resin sites and thus cause a reduction in the actual capacity of the resin . Table VIII presents a typical composition of flyash material recovered from the UTSI MHD facility. The basis for the material balance was chosen as $111147 \frac{lbs}{hr}$ of K_2SO_4 being fed since several other seed regeneration processes previously investigated [20], used this value as the basis. With this basis in hand, the first step in the process is to

Table VII.

Design Basis for Proposed Seed Regeneration Plant [1].

MHD Plant Size	1000 MW_e
Overall MHD Plant Efficiency	44% (2273 MW_t)
MHD Plant Life	30 years
Maintenance Cost	5% of equipment costs/year
Type of Coal	Illinois #6 dried to 2% moisture as fired
Potassium Flow Rate	1% of total primary gas flow
Oxygen Enrichment	34 molar % O_2
Stoichiometric Ratio	0.85 (primary)

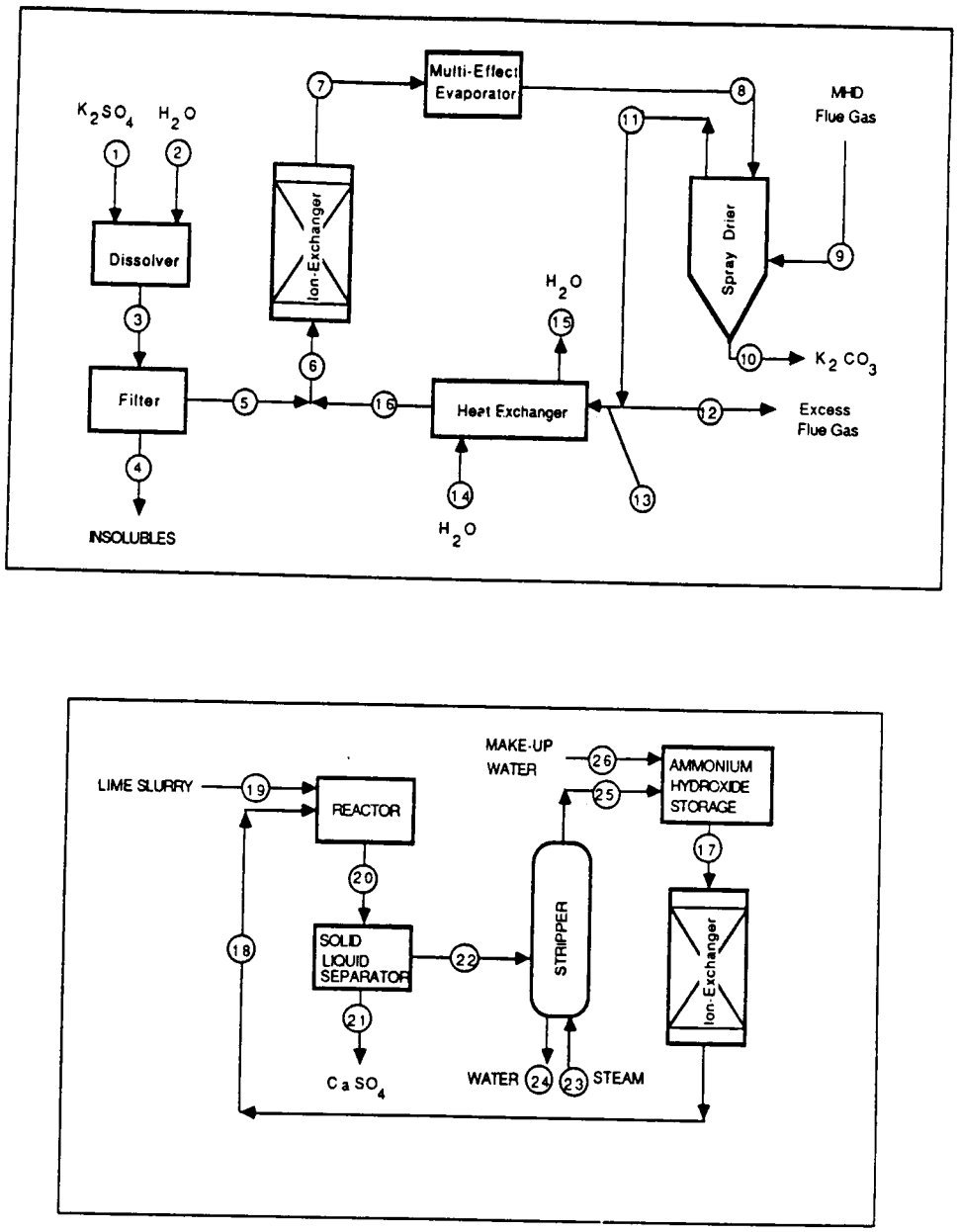


Figure 22. Schematic diagram of proposed seed regeneration plant

Table VIII.

Chemical Composition of the Spent Seed Extract [1]

Major Cations/Elements	Concentration (ppm)
Silicon:	5
Aluminum:	5
Iron:	0.1
Titanium:	Not Detected
Calcium:	112
Magnesium:	10
Sodium:	81
Potassium:	15300
Major Anions	**Concentration (ppm)**
SO_4^{2-}	18800
Cl^-	50
F^-	31

obtain the proper design parameters needed for the material balance calculations. The most important of these parameters is the equilibrium capacity of the resin at a given pressure. This value determines how much sulfate can be removed from the solution and also allows for calculation of the amount of resin required for the operation. The next step in the process is to determine the initial concentration of the feed solution to the ion-exchange columns. This concentration value is important because it dictates much of the water requirements for the dissolver unit of the seed regeneration plant. If a high concentration is chosen, less water is required; however, the bed is exhausted much faster and the time between successive regeneration of the bed becomes shorter. Low concentrations ,on the other hand, means very high water and energy requirements which might add to the size of the evaporator and dryer and thus increase the cost of the plant. Based upon the above considerations the initial concentration chosen was 120,000 ppm which is the solubility limit of K_2SO_4 at $25°C$. For this value of the inlet concentration and at a pressure of 20 psig, the equilibrium capacity of the resin is .0867 $[\frac{gms SO_4^{2-}}{ml.resin}]$.

The proposed seed regeneration process is based on the continuous processing of spent seed using multiple ion-exchange columns. The ion-exchange resin-based seed regeneration process begins at the spent-seed recovery units of the MHD flow train. At this point, spent-seed material recovered from the baghouse and electrostatic precipitator are placed in a storage tank. From the storage tank, the spent seed is conveyed to the dissolver where it is mixed with water to form a solution of desired concentration. Any undissolved solids are then removed in the filtration step. The insoluble solids are discarded or recycled to the optional lime digestion step (not included here), while the filtrate is pumped to the ion-exchange columns. Multiple ion-exchange columns are used to facilitate simultaneous exhaustion and

regeneration of the resin. The evaporation and spray drying units downstream of the ion-exchange columns will be used for decomposition and concentration of the $KHCO_3$ solution produced from the ion-exchange operation. The decomposition of the $KHCO_3$ is described by the following reaction.

$$2KHCO_3 \longrightarrow K_2CO_3 + CO_2 + H_2O \tag{45}$$

Any water remaining in the concentrated carbonate solution is removed in the spray dryer which is fed with hot flue gases coming from the MHD plant. The flue gases also provide the necessary CO_2 required for pressurization of the ion-exchange column and carbonation of the regenerated resin to its bicarbonate form. A heat exchanger is added at the spray dryer outlet to cool the the flue gases before they reach the ion-exchange column. A summary of the results from the material balance calculations are shown in Tables IX and X. All assumptions used in the calculations are given in Table XI.

Preliminary Economics

Using the results obtained from the material balance, a preliminary cost analysis of the ion-exchange resin-based seed regeneration plant was completed by the Resources Conservation Company [23]. All costs are expressed in early 1988 dollars. Prices for major equipment items such as the evaporator, spray drier, and ion-exchange columns were quoted by suppliers. Other equipment was costed parametrically using Peter's and Timmerhaus [21] or Perry [22] and updated to 1988 dollars using the chemical engineering equipment cost index. Installed cost, where estimated parametrically were taken as 200% of equipment cost [23]. Table XII gives values for the initial capital investment for the proposed seed regeneration plant. The operating costs of the plant were calculated for plant

Table IX.

Summary of Material Balance Calculations ‡ (lbs./hr.)

STREAM	K_2SO_4	H_2O	$KHCO_3$	K_2CO_3	CO_2	N_2	O_2
1	111147						
2		929939					
3	111147	929939					
4							
5	111147	929939					
6	111147	929939			61758	97365	2366
7	111147	847248	127712		6175.8	97365	2366
8		88154		88154	34247.8	97365	2366
9					189173	352234	8559
10		88154		88154		352234	8559
11					189173	352234	8559
12					161662	254869	6193.15
13					61758	97365	2366
14		98483				97365	2366
15		98483					
16					61758	97365	2366

‡ Material balance for exhaustion step

Table X.

Summary of Material Balance Calculations † (lbs./hr.)

STREAM	$Ca(OH)_2$	$CaSO_4$	H_2O	NH_4OH	$(NH_4)_2SO_4$	NH_3	Steam *
17			514142	44708			
18			514142		84328		
19	47201		424814				
20		86787	938956			21711	
21		86787	97866				
22			864078			21711	
23							203572
24			55828				
25			864078				21711
26			193848				

* Steam supplied at 77 ^oF and 240 psia.
† Material balance for regeneration step

Table XI.

Assumptions for Material Balance and Cost Analysis [23]

- Calculations are based on 111147 lbs/hr K_2SO_4 fed.
- Plant operation is 350 days/yr. and 24 hrs/day.
- Potassium bicarbonate will decompose completely in the multi-effect evaporator at temperatures above $60°C$ to K_2CO_3
- Cost of ion-exchange colums calculated for six columns: The column dimensions are ($16.5ft.$ diameter, $33ft.$ high)
- Cost of CO_2 determined based on the enthalpy value of the thermal content of the flue gas.
- Engineering and supervision costs are 20% of capital cost.
- Construction and expense fee 12% of direct cost.
- Maintenence cost are calculated as 6% of capital cost
- No allowance is made for depreciation, plant overhead and administration costs.

Table XII.

Initial Capital Costs for the Proposed Seed Regeneration Plant [23]

Equipment	Purchase Price ($)	Installed Cost ($)
Spent seed silo	201,500	421,000
Dissolver	82,800	165,600
Filter	96,600	193,203
Thickener before filter		177,400
Ion-exchangers	2,500,000	2,500,000
Resin		5,722,000
Weak $KHCO_3$ tank	59,300	118,600
Evaporator	5,885,500	13,400,000
Strong K_2CO_3 tank	16,600	33,200
Spray drier	2,000,000	4,000,000
Regenerated seed silo	100,000	200,000
Cooling condenser	2,800	5,600
Recovered H_2O tank	59,300	118,600
Carbon Dioxide receiver	413,900	827,800
Gas blower		1,778,500
NH_4OH tank	38,600	77,200
$(NH_4)_2SO_4$ tank	15,200	30,400
Lime slaker		2,000,000
Lime storage tank	41,400	82,800
Ammonia stripper		584700
Gypsum clarifier		149,600
Clarifier underflow receiver	18,400	36,800
Gypsum centrifuge		494,400
Transfer pumps		332,400
Controls		1,000,000
Engineering site work		10,000,000
Total direct cost		45,382,200
Engineering and supervision		4,538,200
Construction and expense fee		5,445,800
5% Contingency		2,914,000
Total Fixed Cost		58,280,200

uptime of $350\frac{days}{yr.}$ and $24\frac{hrs}{day}$. No allowance was made for fixed charges, plant overhead, administrative costs, or financing. Labor costs were calculated from Figure 4-8 of Peters and Timmerhaus [21]. The cost of steam was taken as \$1.38 per 1000 lbs and the cost of process water was estimated to be \$0.25 per 1000 gals. Maintenence cost presented in Table XIII was taken as 6% of the initial capital investment. Table XIII presents annual operating costs in 1988 dollars.

Comparison with Existing Processes

The ion-exchange resin-based seed regeneration concept compares favorably to many of the existing seed regeneration processes when the environmental, economic, and energy considerations for each process are taken into account. The ion-exchange resin-based seed regeneration process poses no serious environmental problems,since the main by-product of the system, calcium sulfate, is a relatively harmless waste product and easily disposable. Ammonia which is produced along with the calcium sulfate is stripped to produce ammonium hydroxide which can be used in the resin regeneration cycle. Other seed regeneration processes such as the PERC Process, the Aqueous Carbonate Process, and the Modified Tampella Process recover sulfur in a salable form such as elemental sulfur or H_2SO_4, however, they require high temperature reduction of sulfate. The Engel-Precht, Formate and Double-Alkali Processes require lower temperatures but use relatively complex double decomposition/ precipitation reactions and unproven technology or components to recover the sulfate in a disposable form[24].

The problems posed by the options disscused above make it necessary to give strong consideration to an alternate seed regeneration concept such as ion-exchange resin based seed regeneration. Technically, the ion-exchange system is a relatively simple one when compared to other processes discussed in this study.

Table XIII.

Annual Operating Costs for the Proposed Seed Regeneration Plant [23]

Item	Cost ($)
Steam	5,878,800
Electricity	1,321,200
Cooling Water	767,100
Make-up Water	336,900
Lime	7,282,000
Ammonia	2,260,500
Flue Gas for CO_2	2,983,500
Resin Replacement	1,144,400
Maintenence	3,496,800
Labor	1,966,100
Total Operating Cost	25,107,100

In addition, the sulfur containing by-product of the ion-exchange resin-based option, calcium sulfate poses no serious environmental problems because it contains no $CaSO_3$. Comparison of the fixed and operating costs for the ion-exchange resin-based plant with those of existing processes will provide the most valuable information about its economic feasibility. Table XIV presents fixed cost and annual operating cost for various seed regeneration systems. These results show that the ion-exchange resin-based process is economically competitive. The fixed capital cost of $\approx$ 58,000,000 dollars are competitive with other processes which cause more difficult technical and environmental problems and also use unproven technology or need a lot of developmental efforts.

Table XIV.

Comparison of Economics for Candidate Seed Regeneration Processes

Option*	Capital Costs (MM$)	Annual Operating Costs (MM$)
Type I Process**	60.2 - 105.7	28.0 - 63.7
Type II Process***	46.6 - 125.0	25.2 - 149.3
Ion-Exchange (This Study)	58.3	25.2

* Basis: $1000 MW_e$ MHD plant burning Illinois No. 6 Coal.

** Reduction Based Processes

*** Processes Based on Double Decomposition/Precipitation type reactions

CHAPTER VIII

CONCLUSIONS AND RECOMMENDATIONS

The study of the ion-exchange resin-based seed regeneration process presented in the preceeding chapters yielded information about the behavior of the sulfate-bicarbonate system and also about the economic feasibility of this approach for seed regeneration. Based on the results obtained, it can be said that placing the system under CO_2 pressure resulted in a increase in the equilibrium capacity of the resin. This result can be attributed to a shift in the carbonation reaction which favors production of bicarbonate ions on the active sites of the resin. The Langmuir constant, a_2, obtained from the analysis of the breakthrough data, showed that the exchange reaction was governed by a highly non-linear equilibrium. This is reflected in the much higher values for the Langmuir constant, a_2 (830, 322), obtained from the analysis of the equilibrium data. The Langmuir constant a_2 is equivalent to the equilibrium constant $\overline{K}$, and for values of $\overline{K}$ greater than one the equilibrium of the system is shown to be favorable and non-linear. In addition, the $\frac{D}{R^2}$ values increased with changes in concentration which suggests that increasing the inlet concentration could increase the driving force for diffusion up to certain limits. Application of Antonson's model to describe the breakthrough behavior of the sulfate-bicarbonate system worked fairly well; however, results obtained from work on a similar system by Liberti and Passino [19] suggest, that the assumption of particle side diffusion being the only controlling mechanism might be incomplete. Instead, they suggest that the rate might be controlled by the exchange reaction or a combination of the exchange reaction and a diffusion mechanism.

The economic evaluation of the ion-exchange resin-based seed regeneration plant showed that the process would be competitive with existing options. The

process can operate well under moderate conditions of pressure and temperature, is relatively simple, uses proven technology and may need relatively less development time when compared to current seed regeneration options. Other factors such as low fixed capital and operating costs, no environmentally harmful waste products and high recovery capability make the process very attractive.

Recommendations

The results obtained from the fixed bed experiments have shown that the ion-exchange resin-based seed regeneration concept is an attractive approach for the problem of recovery and recycle of spent seed material from MHD power plants in a sulfur-free form. Before this concept is applied commercially, steps must be taken to improve the technical and economic merits of the proposed system. First, further bench scale experiments need to be carried out to determine if there is a limiting pressure beyond which the equilibrium capacity of the resin either remains unchanged or starts decreasing. This would aid in determining the optimum operating pressure of the system and save on cost of equipment and CO_2. Next, a more complete mathematical model must be developed to predict the breakthrough behaviour of the sulfate-bicarbonate system. This model should be based on an investigation of the sulfate-bicarbonate system to determine what effect the exchange reaction, liquid-side mass transfer and other soluble anions have on the kinetics of the system. This could be accomplished by doing experiments with ion-exchange resins having anions other than HCO_3^- on the active sites. If the rate of the exchange reaction between sulfate and other anions such as NO_3^-, and Cl^-, is significantly different from that of the reaction with the bicarbonate ion, then it is possible that the exchange reaction could indeed be a significant rate controlling step and should be accounted for in the model . In addition, an investigation of the behavior of the system using various particle sizes would show if macropore or micropore diffusion was occuring during the kinetics

of the process. Screening of the various commercially available anion-exchange resins also needs to be carried out to select the best one for this application. Finally, development and operation of a pilot-plant would be of major value in determining the true value of this process.

LIST OF REFERENCES

LIST OF REFERENCES

1. Butler, William A., Master's Thesis, "Bench Scale Evaluation of Anion-Exchange Resin-Based Seed Regeneration Concept for Coal Fired Magnetohydrodynamic Power System, " University of Tennessee Space Institute, Tullahoma, Tennessee (1986).

2. Sheth, A.C., Johnson, T.R., "Evaluation of Available MHD Seed Regeneration Processes on the Basis of Energy considerations" ANL/MHD-78-4, Argonne National Laboratory, Argonne Illinois, 1978.

3. Weber, O.W., *et al.*, "The Absorption of Carbon Dioxide by Weak Base Ion Exchange Resins, " AIChE Journal **16** (4) 609(1970).

4. Burstall E.H., *et al.*, "Ion Exchange Process for Recovery of Gold from Cyanide Solution, " Industrial and Engineering Chemistry, **45** 1648(1953).

5. Rosen J.B., "Kinetics of a Fixed Bed System for Solid Diffusion into Spherical Particles," Journal of Chemical Physics, **20** (3) 387(1952).

6. Ho. Cecilia, *et al.*, "A Comparative Study of Zeolite and Resin Adsorbents for the Separaton of Fructose – Glucose Mixtures," Industrial Engineering Chemistry **26** 1407(1987).

7. Tien, C., Thodos, G., "Ion Exchange Kinetics for Systems of Nonlinear Equilibrium Relationships," AIChE Journal **5**(3) 373(1959).

8. Dranoff, J.S. Griffin, R.P., "The Rate of Glycerol Absorption by Ion Exchange Resins," AIChE Journal **9**(2) 283(1953).

9. Antonson, C.R., Ph.D. Dissertation, "Adsorption of Ethane in Molecular Sieve Particles," Northwestern University, Evanston, Illinois , (1968).

10. Thomas, H.C., "Heterogeneous Ion Exchange in a Flowing System," Journal of the American Chemical Society, **66** 1644(1944).

11. Heister, N.K., Vermeulen, T. "Saturation Performance of Ion Exchange and Adsorption Columns," Chemical Engineering Progress , **48** 505(1952).

12. Chong Sho Chemical Fraternity, " Application of Ion Exchange Technique in Seed Regeneration Experiments for MHD Power Generation," Su Chow Area Chemical Institute, China, 1980.

13. Carberry, James J., Chemical and Catalytic Reaction Engineering, McGraw-Hill Book Company, New York, 1976.

14. Hall, *et al.* "Pore- and Solid-Diffusion Kinetics in Fixed-Bed Adsorption under Constant-Pattern Conditions," Industrial and Engineering Chemistry Fundamentals, **5**(2) 1966.

15. Rohm & Haas Technical Bulletin, "Amberlite IRA-68 Technical Notes," Rohm & Haas Company, 1979.

16. Colwell,C.J., Ph.D. Dissertation, Northwestern University, "The effects of Non-linear Equilibrium and Axial Dispersion in Ion Exclusion, "Evanston, Illinois,1968.

17. Reid, *et al.* The Properties of Gases and Liquids, 3rd. ed., McGraw-Hill Book Company, New York, 1977.

18. Marinsky, Jacob A., Marcus, Y., editors, "Ion exchange Kinetics in Selective Systems, " Ion Exchange and Solvent Extraction **9** 175(1985).

19. Bonhoeffer, K.F.,*et al.*, Z. Phys. Chem., **198** 270(1951).

20. Jackson, D.M., "Evaluation of Seed Regeneration Processes for Coal-Fired MHD Power Plants," FE-1760-36 a report prepared by the University of Tennessee Space Institute for DOE under Contract No. DE-AC02-79ET10815, 1985.

21. Peters, M.S., Timmerhaus, K.D., Plant Design and Economics for ChemicalEngineers 2nd. ed., McGraw-Hill Book Company, New York, 1980.

22. Perry, Robert H., Chilton, C.H. Chemical Engineer's Handbook, 5th ed., McGraw-Hill Book Company, New York, 1973.

23. A private communication with Resources Conservation Company, Bellevue, Washington 1988.

24. Sheth, A.C. *et al.* "Anion-Exchange Resin-Based Desulfurization Process for Alkali Metal Sulfates," Proceedings: 26th Symposium on Engineering Aspects of Magnetohydrodynamics, Nashville, Tennessee, 1988.

25. Garg, D. R., Ruthven, D. M., Chemical Engineering Science **29** 571(1974).

26. Selke, W. A., Bliss, H., "Application of Ion Exchange, Copper-Amberlite IR-120 in Fixed Beds," Chemical Engineering Progress **46** 509(1950).

27. Sheth A. C., Master's Thesis, "Kinetics of Ethylene Adsorption-Desorption on Molecular Sieves," Northwestern University, Evanston, Illinois, 1969.

APPENDIXES

APPENDIX A

COMPUTER SCHEME

COMPUTER SCHEME

This section will present an overview of the finite difference technique used to get ϕ as a function of θ^*. The method used is the same as that presented and developed by Antonson [9] in his molecular sieve studies. Beginning with the integro-differential equation (36) presented in Chapter III, the integration can be divided into a series of integrations over small intervals of size $\Delta\theta^*$. Applying the second mean value theorem of the calculus would then yield:

$$\frac{\partial\phi}{\partial X^*} = -2\sum_{n=1}^{\infty}\sum_{g=0}^{M}\frac{\partial\phi}{\partial\lambda}\bigg|_{g+\alpha l}\int_{gl}^{(g+1)l} exp(-\frac{1}{2}n^2\pi^2(\theta^* - \lambda))d\lambda \qquad (A-1)$$

where,

$$0 < \alpha < 1$$

$$M = \frac{(\theta^* - l)}{l}$$

$$l = \Delta\theta^*$$

$$f(\phi) = \frac{\phi}{1 + a_2 C_o \phi}$$

Defining $\phi(i,g) = \phi(i\Delta X^*, g\Delta\theta^*)$, $f(i,g) = f(\Delta X^*, g\Delta\theta^*)$ and $h = \Delta X^*$ will yield the following finite difference approximations:

$$\frac{\partial\phi}{\partial X^*} \simeq \frac{\phi(i+1, M+1) - \phi(i, M+1)}{h} \qquad (A-2)$$

$$\left.\frac{\partial\phi}{\partial\lambda}\right|_{g+\alpha l} \simeq \frac{\phi(i+1,g+1)-\phi(i+1,g)}{l} = \frac{DER(i+1,g)}{l} \qquad (A-3)$$

Substituting (A-2) and (A-3) into equation (A-1) and carrying out the integration will result in the following expression for the concentration $\phi(i+1,M+1)$:

$$\phi(i+1,M+1) = \phi(i,M+1) - 4h\sum_{n=1}^{\infty}\sum_{g=0}^{M}\frac{DER(i+1,g)}{n^2\pi^2 l} \\ exp(-\frac{1}{2}n^2\pi^2 l(M-g)) - exp(-\frac{1}{2}n^2\pi^2 l(M+1-g)) \qquad (A-4)$$

A more convenient way of expressing the equations presented above is possible since the term $DER(i+1,M)$ is a function of the concentration ϕ:

$$DER(i+1,M) = \left[\frac{\phi(i+1,M+1)}{(1+a_2C_o\phi(i+1,M+1))} - \frac{\phi(i+1,M)}{(1+a_2C_o\phi(i+1,M))}\right] \qquad (A-5)$$

$$\phi(i+1,M+1) = \phi(i,M+1) - 2hEE(l)\frac{\phi(i+1,M+1)}{(1+a_2C_o\phi(i+1,M+1))} \\ - \frac{\phi(i+1,M)}{(1+a_2C_o\phi(i+1,M))} - 4h\sum_{n=1}^{\infty}\sum_{g=0}^{M}\frac{DER(i+1,g)}{n^2\pi^2 l} \\ \left\{exp(-\frac{1}{2}n^2\pi^2 l(M-g)) - exp(-\frac{1}{2}n^2\pi^2 l(M+1-g))\right\} \qquad (A-6)$$

where EE(l) is given by:

$$EE(l) = \sum_{n=1}^{\infty} \left[\frac{1 - exp(-\frac{1}{2}n^2\pi^2 l)}{n^2\pi^2 l} \right] \qquad (A-7)$$

The values of $EE(l)$ can be approximated via an expression derived by Paterson [9]:

$$EE(l) \simeq -\frac{1}{2} + \frac{2}{\pi l} \qquad (A-8)$$

Equation (36) can be further simplified was affected by rewriting the double summation as a recursive relationship:

$$\sum_{n=1}^{\infty} S_n(M-1) = 2\sum_{n=1}^{\infty}\sum_{g=0}^{M-1} \frac{DER(i+1,g)}{n^2\pi^2 l} \left\{ exp(-\frac{1}{2}n^2\pi^2 l(M-g)) - exp(-\frac{1}{2}n^2\pi^2 l(M+1-g)) \right\} \qquad (A-9)$$

where,

$$S_n(M-1) = S_n(M-2)exp(-\frac{1}{2}n^2\pi^2 l) + 2\frac{DER(i+1,M-1)}{n^2\pi^2 l} \left\{ exp(-\frac{1}{2}n^2\pi^2 l) - exp(-n^2\pi^2 l) \right\} \qquad (A-10)$$

and $S_n(-1) = 0$. The recursive technique presented above was first applied by Colwell [16] for the generation of breakthrough curves. The advantage of this scheme is that it allows $S_n(M-1)$ to converge in a finite number of terms, N. Applying this technique to equation (A-6) gives:

$$\phi(i+1,M+1) = \phi(i+1,M) - 2h\sum_{n=1}^{N} S_n(M-1) - 2hEE(l)\frac{\phi(i+1,M+1)}{(1+a_2C_o\phi(i+1,M+1))} - \frac{\phi(i+1,M)}{(1+a_2C_o\phi(i+1,M))} \quad (A-11)$$

Finally, placing equation (A-10) into a second order polynomial permits easy evaluation of the concentration $\phi(i+1,M+1)$:

$$\phi^2(i+1,M+1) + \beta\phi(i+1,M+1) - \gamma^* = 0 \quad (A-12)$$

$$\phi(i+1,M+1) = \frac{(-\beta + (\beta^2 + 4\gamma^*)^{\frac{1}{2}})}{2} \quad (A-13)$$

where γ^* and β are given by:

$$\gamma^* = \left\{ \frac{\phi(i,M+1) - 2hEE(l)\left[\frac{\phi(i+1,M)}{(1+a_2C_o\phi(i+1,M)}\right] - 2h\sum_{n=1}^{N} S_n(M-1)}{a_2C_o} \right\} \quad (A-14)$$

$$\beta = \frac{-(\gamma^* a_2 C_o) + ((1+2hEE(l))}{a_2C_o} \quad (A-15)$$

It must be noted that for the case of linear equilibrium, the finite difference scheme is also linear. In this case, $f(\phi) = \phi$ and the expressions for f are given by:

$$\begin{aligned} \frac{\partial\phi}{\partial\lambda} &\simeq \frac{\phi(i+1,g+1) - \phi(i+1,g)}{l} \\ &= \frac{\phi(i+1,g+1) - \phi(i+1,g)}{l} \\ &= \frac{DER(i+1,g)}{l} \end{aligned} \quad (A-16)$$

and the concentration for the linear case is given by:

$$\phi(i+1,M+1) = \left[\frac{\phi(i,M+1) + 2hEE(l)\phi(i+1,M) - 2h\sum_{n=1}^{N} S_n(M-1)}{1+2hEE(l)}\right] \qquad (A-17)$$

The boundary condition for equations (A-11) and (A-17) are then $\phi(0,M) = 1$ for $M = 1,2,3,...$ and the initial condition is $\phi(i,0) = 0$ for $i = 1,2,3,...$.

The numerical method presented in this section was the basis for a computer code (Appendix B) developed by Antonson for the purpose of generating theoretical breakthrough curves for fixed bed systems with non-linear equilibrium.

APPENDIX B

COMPUTER PROGRAMS

```
      PROGRAM math_model
     NAMELIST /CONTROL/ KK,N,M2,IH,EL,CUT,
      XZERO,I1,I2,K2,NJ,CON,
     *  /THETA/ EE,/XINC/ HINC
      DIMENSION PHI(3,1000),TAU(1000),HINC(20),
      DE(20,170),E(20,170),
     1  EE(20),NN(20),S(170),EL1(20)
       OPEN(UNIT=8,STATUS='OLD')
      READ(8,CONTROL)
      READ(8,THETA)
      CLOSE(UNIT=8)
      OPEN(UNIT=10,STATUS='OLD')
      READ(10,XINC)
      CLOSE(UNIT=10)
C
C     ****************************
C      CALCULATION OF INITIAL AND
C      BOUNDARY CONDITIONS FOR PHI
C     ****************************
C
      PHI (2,1)=0.
      PI=3.14592654
      PSI = PI*PI/2.
C
      DO K = 1,KK
      PHI(2,K)=0.0
      ENDDO
      IF (I2-1) 9,9,8
    8 READ (25,*)(PHI(1,K),K=2,KK)
      GO TO 11
    9 DO K=2,KK
      PHI(1,K)=1.0
      END DO
C
C     ***********************************
C      CALCULATION OF PARAMETERS FOR USE
C      IN THE FINITE DIFFERENCE SCHEME
C     ***********************************
C
   11 DO J=1,N
      DE(1,J)=EXP(-PSI*(J**2)*EL)
      E(1,J)=(1.0-DE(1,J))/(EL*PSI*(J**2))
      END DO
      OPEN (UNIT=15, STATUS='NEW')
      OPEN (UNIT=16, STATUS='NEW')
      OPEN (UNIT=17, STATUS='NEW')
      OPEN (UNIT=18, STATUS='NEW')
      WRITE (15,105)1,N,EE(1),(DE(1,J),
      J=1,N),(E(1,J),J=1,N)
      NN(1)=N
      EL1(1)=EL
      DO L=2,M2
      EL1(L)=EL1(L-1)*2
      NN(L)=(NN(L-1)*23)/32
      N10=NN(L-1)
      DO J=1,N10
      DE(L,J)=DE(L-1,J)**2
      E(L,J)=(1.0-DE(L,J))/(PSI*EL1(L)*(J**2))
      END DO
```

```
      WRITE (15,105)L,NN(L),EE(L),(DE(L,J),
      J=1,N10),(E(L,J),J=1,N10)
      END DO
C
C     ****************************
C     CALCULATION OF THE TIMES AT
C     WHICH PHI(2,I) IS WRITTEN OUT
C     ****************************
C
      TAU(1)=0.0
      DO K=6,KK,5
      I=((K-6)/30)+1
      IF (I-M2) 15,15,14
   14 I=M2
   15 TAU(K)=TAU(K-5)+5.*EL1(I)
      END DO
      WRITE(15,103)(TAU(K),K=1,KK,5)
      NI=1
      I=I1
      K1=K2
      X=XZERO
      H=HINC(1)
C     ************************************
C     BEGINNING OF FINITE DIFFERENCE SCHEME
C     ************************************
C
   18 DO J=1,N
      S(J)=0.
      END DO
      SUM=0.
      X=X+H
      XLANG=0.
C
      DO K=K1,KK
      C=(PHI(1,K)+2.*H*EE(I)*XLANG-2.*H*SUM)/CON
      B=-(C*CON)+((1.+2.*H*EE(I))/CON)
      PHI(2,K)=(-B+SQRT((B**2)+4.*C))/2.
      IF (PHI(2,K)-1.E-7) 20,21,21
   20 PHI(2,K)=0.
      K2=K+1
   21 XMUIR=(PHI(2,K)/(1.+CON*PHI(2,K)))
      DERV=XMUIR-XLANG
      XLANG=XMUIR
      P=((K-1)/30.)+1.
      IF (P-M2) 23,23,22
   22    NK=M2
      I=NK
      GO TO 26
   23 Q = INT(P)
      IF (P-Q) 24,24,25
   24 NK=I-1
      GO TO 26
   25 NK=1
   26 N10=NN(NK)
```

```
      SUM =0.
      DO J=1,N10
      S(J)=(S(J)+DERV*E(NK,J))*DE(I,J)
      SUM=SUM+S(J)
      END DO
      END DO
      WRITE (18,106)X,K1,(PHI(2,K),K=1,KK,5)
C
C     ************************
C     PREPARATION FOR NEXT STEP
C     IN THE X-2 DIRECTION
C     ************************
C
      K1=K2
      I = ((K2-2)/30)+1
      IF (I-M2) 32,32,29
   29 I=M2
   32 IF (NI-IH) 31,30,30
   30 NI=IH
      GO TO 36
   31 NI=(NJ/30)+1
      NJ = NJ+1
   36 H=HINC(NI)
      IF (X-CUT) 33,35,35
   33 DO K=K1,KK
      PHI(1,K)=PHI(2,K)
      END DO
      GO TO 18
   35 CONTINUE
      WRITE(25,109)(PHI(2,K),K=2,KK)
      CLOSE(UNIT=15)
      CLOSE(UNIT=16)
      CLOSE(UNIT=17)
      CLOSE(UNIT=18)
C
  100 FORMAT(2I4,3I2,3F10.7,4I4,E8.1)
  101 FORMAT(7F11.7)
  102 FORMAT(8F10.8)
  103 FORMAT(1H1,3HTAU/(4X,10F10.5))
  105 FORMAT(//3H L=,I2,5X2HN=,I3,
      5X9HZERO-SUM=,E18.10/(9X,10F11.8))
  106 FORMAT(////10H DISTANCE=,F10.6,
      10X3HK1=,I4//(9X10F11.8))
  109 FORMAT(8F10.7)
      END
```

```
      IMPLICIT REAL*8(A-H,O-Z)
      NAMELIST /TIME/ X, /CONC/ Y
      DIMENSION X(18),Y(18)
C     ************************************
C     THIS PROGRAM WILL CALCULATE THE AREA
C     UNDER THE BREAKTHROUGH CURVE AND THE
C     EQUILIBRIUM CAPACITY, USING THE
      TRAPEZOIDAL METHOD
C     ************************************
      OPEN(UNIT=21, STATUS = 'OLD')
      READ(21,TIME)
      READ(21,CONC)
      CLOSE(UNIT=21)
      N=18
      DO I = 1,18
      WRITE(5,*)I,X(I),Y(I)
      ENDDO
      NINT=N-1
      AREA=0.
      DO  I = 1,NINT
      AREA = AREA + (Y(I)+Y(I+1))*(X(I+1)-X(I))/2.
      WRITE(5,*)'******** AREA IS NOW',AREA
      END DO
      WRITE (5,*) 'THE AREA IS',AREA
      TYPE*,'PLEASE INPUT THE FLOW RATE ,IC, AND RESIN VOL'
      ACCEPT*, FLOW,C,RV
      CAP = FLOW*AREA*C/RV
      WRITE(5,*)'THE CAPACITY IS ',CAP
      STOP
      END
```

APPENDIX C

EXPERIMENTAL DATA

EXPERIMENTAL DATA

Run IEX-1

$\frac{C}{C_o}$	time (mins)	Volume (ml.)	Bed volumes*
0	4.5	225	2.29
.019	12.1	605	6.17
.172	19.5	975	9.95
.601	27.1	1355	13.826
.858	34.4	1720	17.55
.941	42.02	2101	21.43
.982	49.0	2450	24.99
1.0	53.87	2693	27.48

Run IEX-2

$\frac{C}{C_o}$	time (mins)	Volume (ml.)	Bed volumes
0	3.98	199	2.03
011	6.01	300	3.06
.083	8.00	400	4.08
.501	10.02	501	5.11
.843	12.00	600	6.12
.970	13.95	697	7.11
.985	16.01	800	8.16
1.0	18.01	900	9.18

$$* \quad \text{Bed volumes} = \frac{\text{Volume of liquid through bed at time t}}{\text{Volume of resin in bed}}$$

Run IEX-3

$\frac{C}{C_o}$	time (mins)	Volume (ml.)	Bed volumes
0	0	0	0
.025	1.68	84	.857
.201	2.73	136.5	1.39
.693	3.70	185	1.88
.927	4.66	233	2.37
.981	5.70	285	2.90
1.0	7.00	350	3.57

Run IEX-4

$\frac{C}{C_o}$	time (mins)	Volume (ml.)	Bed volumes
0	.50	25	.255
.015	1.8	90	.918
.221	2.76	138	1.408
.954	3.78	189	1.92
.977	4.8	240	2.44
1.0	5.0	250	2.55

Run IEX-5

$\frac{C}{C_o}$	time (mins)	Volume (ml.)	Bed volumes
.009	19.5	2340	11.93
.041	25.0	3000	15.3
.147	30.1	3619	18.46
.338	34.9	4195	21.4
.560	40.0	4802	24.5
.794	44.9	5372	27.4
.918	50.0	6000	30.6
.988	55.1	6612	33.7

Run IEX-6

$\frac{C}{C_o}$	time (mins)	Volume (ml.)	Bed volumes
0	0	0	0
.0131	4.2	504	2.57
.0264	5.94	712	3.63
.054	7.81	937	4.78
.633	10.0	1201	6.12
.918	12.0	1440	7.34
.974	13.0	1562	7.97
1	14.0	1680	8.57

Run IEX-7

$\frac{C}{C_o}$	time (mins)	Volume (ml.)	Bed volumes
0	0	0	0
0	3.27	393	2.00
.121	4.30	516	2.63
.523	5.32	638.2	3.25
.933	6.26	751.2	3.83
.959	7.31	877.2	4.47
1.0	8.34	1000.8	5.10

Run IEX-8

$\frac{C}{C_o}$	time (mins)	Volume (ml.)	Bed volumes
0	2.18	261.6	1.33
.021	2.71	325.2	1.65
.118	3.20	384	1.95
.538	3.69	442.8	2.25
.862	4.2	504	2.57
.976	5.18	621.6	3.17
1.0	6.5	780	3.97

VITA

David Christopher Modeste was born in New Amsterdam, Guyana on April 13th 1963. From September 1974 he attended North Georgetown Secondary School, and in 1977 moved to Knoxville Tennessee completing his high school education at Bearden High School. Upon graduation from Bearden in June 1981, he entered the University of Tennessee at Knoxville and graduated with a Bachelor of Science Degree in Chemical Engineering. In March 1986, he entered the University of Tennessee Space Institute in the Department of Chemical Engineering.